Volume 94, Number 5, September–October 1989
Journal of Research of the National Institute of Standards and Technology

Contents

Articles

Errata

Conference Reports

Volume 94, Number 5, September–October 1989
Journal of Research of the National Institute of Standards and Technology

News Briefs

Volume 94, Number 5, September-October 1989
Journal of Research of the National Institute of Standards and Technology

Volume 94, Number 5, September–October 1989
Journal of Research of the National Institute of Standards and Technology

Instrument-Independent MS/MS Database for XQQ Instruments: A Kinetics-Based Measurement Protocol

Volume 94 Number 5 September–October 1989

Richard I. Martinez

National Institute of Standards and Technology,
Gaithersburg, MD 20899

A detailed kinetics-based measurement protocol is proposed for the development of a standardized MS/MS database for XQQ tandem mass spectrometers. The technical basis for the protocol is summarized. A CAD database format is proposed.

Key words: CAD; CBRIS; characteristic branching ratios of ionic substructures; collisionally-activated dissociation; database; ion-molecule kinetics; measurement protocol; MS/MS; NIST-EPA International Round Robin; spectral library; standardization; tandem mass spectrometers; XQQ instruments (QQQ, BEQQ, etc.).

Accepted: June 5, 1989

1. Introduction

Tandem mass spectrometry (MS/MS) is widely used for structure elucidation and for the analysis of multicomponent mixtures [1]. The analysis makes use of the collisionally-activated dissociation (CAD) of "parent" ions. A parent ion may be a molecular radical cation, a protonated molecule, or a "progeny" fragment ion (daughter, granddaughter, etc. produced by the fragmentation of a larger precursor parent ion). The MS/MS technique consists of three steps: (i) a parent ion is mass selected by the first mass analyzer (designated MS-I); (ii) the selected parent ion collides with a target gas which is located within a reaction region between MS-I and the second mass analyzer (designated MS-II); and (iii) the undissociated parent ions and the progeny fragment ions which were produced within the reaction region are channeled into MS-II for mass analysis. MS/MS instruments thus produce a CAD spectrum of each initially-selected parent ion.

Reference [1] provides an excellent up-to-date review of the capabilities and advantages of the MS/MS technique. Among the advantages enumerated in [1] for MS/MS are:

(a) the functional group specificity of neutral loss experiments (for which there is no analogue in GC/MS) provides the unique ability to rapidly screen unknown mixtures for compound classes (e.g., nitroaromatic cations can be inferred by their loss of NO).

(b) the ability to perform very rapid analyses of targeted compounds in complex mixtures based on unique progeny ions (especially when "soft" ionization techniques are used) or on neutral loss experiments [e.g., the nitroaromatics screened above in (a)], thus avoiding the need to identify every component.

(c) very low limits of detection ($\leqslant$ppt; better than a single stage of mass spectrometry) can be attained with enhanced signal/noise ratios be-

cause of the elimination of "chemical noise" [1].

(d) unstable or extremely reactive species, which cannot be studied directly by optical spectroscopies, NMR, or GC/MS, have been studied directly by MS/MS (e.g., radical trapping of polyatomic free radicals; neutralization-reionization mass spectrometry [1]; etc.).

In principle, standard CAD spectra of a variety of ions (fragment ions, molecular ions, protonated molecules, etc.) could be generated and collected as reference libraries, to be used for comparison against unknown spectra in a manner analogous to the use of reference libraries in the data handling systems of ordinary electron impact mass spectrometers. Further, it should be possible to infer the identity of an unknown molecule by identifying the ionic substructures of fragment ions generated in its CAD spectrum. However, to date reference libraries of CAD spectra have not been collected because of a lack of standardization of operating conditions of MS/MS instruments [1].

This paper addresses the standardization of one of the major classes of commercially-available analytical MS/MS instruments, the so-called "XQQ" tandem mass spectrometers (there are currently more than 400 XQQ MS/MS instruments worldwide, representing a capital investment in excess of $170 million). XQQ instruments have three components: X1 Q2 Q3. X1 designates the first mass analyzer, which can be a quadrupole mass filter (represented by a Q), a reversed-geometry magnetic/electrostatic sector instrument (represented by BE), etc. Q2 designates a quadrupole mass filter operated with only radiofrequency (rf) potentials [no direct current (dc) potentials are used]. Q2 contains the target gas, and provides efficient ion containment of parent ions and of progeny fragment ions. Q3 stands for the second mass analyzer, a quadrupole mass filter.

Because XQQ instruments (QQQ, BEQQ hybrid, etc.) are complex ion-optical devices [2]–[9], the observed spectra can be extremely dependent on the experimental parameters used during the analysis. That is, one observes instrument-dependent CAD spectra. This was clearly demonstrated in a 1983 international round robin [10] wherein very different CAD spectra were observed for the same molecule. That is, the relative intensities measured in different QQQ instruments for any given pair of progeny ions differed by factors ranging into the hundreds, even though the same *nominal* operating conditions were supposedly used in each of the QQQ instruments. Therefore, until now it has not been possible to use a CAD spectrum of a given species in one XQQ instrument to identify and quantitate that same species in a different XQQ instrument.

To develop an instrument-independent MS/MS database (or library) for XQQ instruments, instrument users must be able to tune their instruments to obtain undistorted, dynamically-correct (i.e., instrument-independent) representations of any reactions studied within such instruments [9]. That is, the measurements must be substantially free from kinetic interferences (viz., every effort must be made to ensure a well-defined gas target and to prevent back reactions, impurity reactions, scattering losses, fringing fields, mass discrimination, etc.). The branching-ratio measurements must be precise and accurate ($\pm 10\%$).

Recent work from this laboratory has explored the prerequisite conditions for obtaining instrument-independent dynamically-correct branching ratios for the CAD of ions within XQQ instruments [9]. In this paper a kinetics-based measurement protocol is described for the determination of standard CAD spectra within XQQ instruments. The technical basis for the protocol is summarized. Table 1 includes a typical CAD spectrum measured using this protocol.

This protocol can also be used for the development of a standardized MS/MS database for XQQ instruments. One of the goals of this paper is to promote discussion about the database format best suited to the needs of the analytical mass spectrometry community. The spectrum of table 1 illustrates the database format proposed here. The precepts of the protocol are also applicable to other types of tandem mass spectrometers which have strong focusing properties (e.g., quadrupole-hexapole-quadrupole MS/MS), so long as the energy range used for the pertinent ion chemistry is the same as for XQQ instruments.

The kinetics notation and nomenclature developed in reference [9] are used throughout this paper.

2. General Background

As has been demonstrated [11]–[16], dynamically-correct branching ratios can be measured in XQQ instruments when the key MS/MS instrument parameters [9] are properly selected to account for reaction-induced mass discrimination [9] within Q2 and the intrinsic mass discrimination within the Q3 mass analyzer.

Table 1. Proposed CBRIS[1] database format[2,3]

Parent Ion: $C_2H_3O^+$ (m/z 43)[4,5] Notes: 9, 99, 999[6]
Source Compound: 2,3-butanedione (99.9%)
Ionization Mode: 70 eV electrons

E_{CM} (eV)	σ (Å^2)	$\propto$ (13^+)	β (14^+)	γ (15^+)	δ (26^+)	ϵ (27^+)	ζ (28^+)	η (29^+)
2.4	15 [20]	0	0	0.999 [2]	0	0	0	0.0010 [50]
19.3	22 [10]	0.0127 [15]	0.0493 [6]	0.915 [2]	0.0101 [7]	0.0013 [10]	0.0005 [35]	0.0114 [7]
38.6	21 [10]	0.0227 [10]	0.0750 [6]	0.839 [2]	0.0436 [6]	0.0055 [20]	0.0055 [20]	0.0086 [15]

[1] CBRIS=Characteristic Branching Ratios of Ionic Substructures.
[2] For this example we show the branching ratios ($\propto -\eta$) vs the center-of-mass collision energy (E_{CM}) for the CAD of ($C_2H_3O^+$) from the source compound biacetyl [16].
[3] The numbers in the square brackets represent the maximum uncertainty in the cross section σ and in the branching ratios ($\propto -\eta$), expressed as a percentage of each σ and of each branching ratio {e.g., for biacetyl at E_{CM}=2.4 eV, the maximum uncertainty in γ is $\pm([2\%]/100)\gamma$; i.e., $\gamma=0.999\pm0.02$}.
[4] A reference citation would be provided for each CAD spectrum to identify the source of the data.
[5] For the CAD of any given parent ion (e.g., $C_2H_3O^+$), appropriate corrections must be made for contributions from the concurrent CAD of isobaric ions (e.g., $C_3H_7^+$), regardless of their source. The isobaric ions may be co-produced in the ion source (i) from the source compound (e.g., ionization of $CH_3C(O)C_3H_7$ will produce both CH_3CO^+ and $C_3H_7^+$) and/or (ii) from a neutral impurity in a source compound (e.g., for a butanol impurity in a 2-butanone source compound, the butanol generates $C_3H_7^+$, while the 2-butanone generates CH_3CO^+). Fortunately, the CAD spectra of CH_3CO^+ and $C_3H_7^+$ are easily distinguishable [16]. That is, for the CAD of $C_3H_7^+$, $C_2H_3^+$ (m/z 27) is the major CAD fragment for $E_{CM}\simeq2-80$ eV. By contrast, for the CAD of $C_2H_3O^+$, $C_2H_3^+$ is not produced at E_{CM}=2.4 eV, and is only a very minor fragment for $E_{CM}>2.4$ eV. Unfortunately, even minor impurities can contribute disproportionately to the CAD spectrum of a source compound because of differences in the CAD dynamics of isomeric and/or isobaric ions. Because of this problem, it is advisable that both the source compound and the target gas be of high purity (>99.95%). Otherwise, the impurities must be characterized so that appropriate corrections can be made for their contribution to the observed CAD spectrum.
[6] The *Notes* field would be used to refer a user of the database to any information of special significance about the parent ion (e.g., structure of the ion, etc.). The notes enumerated in all the *Notes* fields of the CBRIS database would be collected together in a separate "Notes Appendix". For the example given here, Notes 9, 99, and 999 would be found in the Notes Appendix, and might contain the following types of information.
Note 9: For a given E_{CM}, the branching ratio for each fragment ion is substantially the same for all CH_3CO-X source compounds (e.g., biacetyl, acetone, acetophenone, etc.) [16]. The reactant ion entering Q2 appears to be pure CH_3CO^+ in every case [16].
Note 99: The energy dependence (magnitude and direction) of the branching ratios is distinctly different for the isobars $C_2H_3O^+$ and $C_3H_7^+$ [16]. Hence, one can readily distinguish $C_2H_3O^+$ from $C_3H_7^+$.
Note 999: One can readily distinguish ethanol, oxirane, and cis-2,3-epoxybutane from each other, and from CH_3CO-X source compounds on the basis of the energy dependence of the branching ratios for the CAD of $C_2H_3O^+$ [16].

The systems studied in this laboratory include charge transfer and dissociative charge transfer reactions, and CAD.

Charge Transfer:

$$Ne^+ + Ne \rightarrow Ne + Ne^+ \quad [11],$$

$$Ar^+ + Ar \rightarrow Ar + Ar^+ \quad [12],$$

and $$Ar^+ + N_2 \rightarrow Ar + N_2^+ \quad [13]$$

Dissociative Charge Transfer:

$$N_2^+ + SF_6 \rightarrow N_2 + SF_x^+ + (6-x)\,F$$

(where $x=1-5$) [14]

CAD:

$$(CH_3)_2CO^+ \xrightarrow{\text{Ar CAD}} CH_3CO^+ + CH_3 \quad [15]$$

$$CH_3CO^+ \xrightarrow{\text{Ar CAD}} CH_3^+ + CO \quad [16]$$

Note that for collision energies $E_{LAB} \simeq 1-200$ eV in the Laboratory (LAB) frame of reference, charge transfer reactions are experimentally equivalent to a "worst-case" CAD reaction system because they take place at large impact parameters with near-zero momentum transfer. That is, the product ions of a charge transfer reaction are formed essentially at rest (thermal energies) within Q2 [17]–[20].

The studies in our laboratory led to the development of a kinetics-based measurement protocol for the generation of standard XQQ spectra. Using the protocol, one can obtain, for the first time, accuracy and precision for CAD measurements within XQQ tandem mass spectrometers. A round robin exercise, the NIST-EPA International Round Robin [21], was organized to ascertain which commercially-available XQQ instruments are capable of generating dynamically-correct (i.e., instrument-independent) spectra. Appendix 1 contains the actual round-robin protocol which was disseminated to 22 laboratories worldwide (including the six XQQ instrument manufacturers). Analysis of the round robin data from six participants indicates that at least 50% of the QQQ instruments which have been sold and are currently in the field can provide such standard spectra [21].

Instruments which can generate dynamically-correct results with the round robin protocol of Appendix 1 can be used to develop a generic, standardized CAD spectral database (or library) based on Characteristic Branching Ratios of Ionic Substructures (CBRIS) (analogous to the use of group frequencies in infrared spectroscopy; see section 5.1). Hence, members of the analytical mass spectrometry community who have such instruments could use the kinetics-based measurement protocol detailed in this paper to generate and contribute instrument-independent CAD spectra of species studied during the course of their work. Contributed CAD spectra (to be sent to this author) would be included in the NIST-EPA Standardized CAD Database currently being developed in our laboratory. The latter would be disseminated by NIST to the analytical mass spectrometry community. To facilitate the critical evaluation of contributed spectra, a dynamically-correct CAD spectrum of a well-studied "model" compound (e.g., n-butylbenzene) should also be submitted.

3. Technical Basis for Protocol

Here we summarize the technical basis for the kinetics-based measurement protocol. For a more detailed treatment, the reader is referred to references [2]–[9].

3.1 Kinetics

With reference to the following general reaction sequence:

$$A^+ + B \rightarrow C^+ + S \qquad (\propto \sigma)$$

$$\rightarrow D^+ + T \qquad (\beta\sigma)$$

etc.

equations (1)–(3) are applicable under pseudo-first order $\{[B]_0 >> [A^+]_0\}$, *single-collision* conditions for a reaction zone of length L wherein the number density of the target gas is [B] and the "target thickness" is $[B]L$. Here σ $(= \propto\sigma + \beta\sigma + ...)$ is the total cross section for the $A^+ + B$ interaction, and the sum of the branching ratios $\propto + \beta + ...$ is equal to 1.

Reactant Ion Decay:

$$\ln Y \equiv \ln \{[A^+]_0/[A^+]\} = \sigma[B]L \qquad (1)$$

and

Product Ion Formation:

$$\ln W_\propto \equiv \ln \{\propto [A^+]_0/(\propto [A^+]_0 - [C^+])\} = \sigma[B]L \qquad (2)$$

$$\ln W_\beta \equiv \ln \{\beta [A^+]_0/(\beta [A^+]_0 - [D^+])\} = \sigma[B]L \qquad (3)$$

etc.

In the case of CAD, A^+ corresponds to the parent ion; B corresponds to the target gas; C^+, D^+, etc. are the progeny fragment ions; and S, T, etc. are the neutral fragments complementary to C^+, D^+, etc.

Under dynamically-correct conditions, the rate of reactant ion decay equals the rate of product ion formation. That is $\ln Y = \ln W_\propto = \ln W_\beta$, etc. Then the product ion intensities C^+, D^+, etc. are related to the extent of consumption of the reactant ion $\{[A^+]_0 - [A^+]\}$ by eqs (4), (5), etc.

$$[C^+] = \propto \{[A^+]_0 - [A^+]\} \qquad (4)$$

$$[D^+]=\beta\{[A^+]_0-[A^+]\} \quad (5)$$

etc.

3.1.1 Dynamically-Correct Representation If the key MS/MS parameters [9] of an XQQ instrument can be tuned so that data generated by the instrument conform to equations (1)-(5) [viz., so that $\alpha+\beta+\gamma+...=1.00$], then the instrument can provide a dynamically-correct representation of any reaction studied within it. That is, by using eqs (4'), (5'), etc., the instrument would provide a measure of the branching ratios equivalent to those that, in principle, would be observed at the scattering center of a molecular beam machine.

$$\alpha=[C^+]/\{[A^+]_0-[A^+]\} \quad (4')$$

$$\beta=[D^+]/\{[A^+]_0-[A^+]\} \quad (5')$$

etc.

3.1.2 Kinetics Constraints The selection of key MS/MS parameter settings is constrained by the kinetics prerequisite for $\alpha+\beta+\gamma+...=1$ (see reference [9]). This prerequisite necessitates that:

(a) each product ion be formed only by the primary reaction (no secondary sources; pseudo-first order, single-collision conditions)
(b) all ions be detected with equal sensitivity (requires Conversion Gain corrections for each detector; see sec. 4)
(c) there be no scattering losses because of unreactive collisions (must have high ion containment within Q2; approximately 100% collection efficiency for product ions and unreacted projectiles)
(d) corrections be made for differences in ion containment (transmission) within the Q2Q3 structure.

3.2 Instrumental Parameters

To accomplish $\alpha+\beta+\gamma+...=1.00$, the key MS/MS parameters must be properly selected to obviate discrimination against product ions because of:

(a) Reaction-Induced Mass Discrimination (RIMD) within Q2 (refer to sec. 3.2.1),
(b) Intrinsic Mass Discrimination (IMD) within Q3 (refer to sec. 3.2.2), or
(c) the kinetic energy of product ions entering Q3 (refer to sec. 3.2.3).

We shall use the terms "RIMD-free" and "IMD-free" to refer to branching ratios α, β, etc. which have been measured in concordance with the precepts detailed next for (a)-(c). That is, to be RIMD-free and IMD-free, the instrument parameters discussed below in sections 3.2.1-3.2.3 have to be tuned and returned iteratively until $\alpha+\beta+\gamma+...\simeq 1.0\pm 0.1$.

3.2.1 Reaction-Induced Mass Discrimination (RIMD) Within Q2 The rf amplitudes of Q1, Q2, and Q3 are characterized here by the Mathieu parameters q_1, q_2, and q_3, respectively (for further information, see references [2]-[5]). In this discussion q^{max}_{react} and q^{max}_{prod} are used to represent, respectively, the values of q_2 which correspond to the maximum ion transmission through Q2Q3 for the reactant (projectile) ion of mass m_{react} and for each product ion of mass m_{prod}. The subscripts "react" and "prod" designate, respectively, the reactant ion A^+ and the product ion C^+ (or D^+, etc.).

Within Q2, $m_{prod}/m_{react}=q_{react}/q_{prod}$ [9]. Therefore, low-mass daughters are not detected when $m_{prod}/m_{react}<q_{react}/0.908$ since ion trajectories are unstable when $q_2>0.908$ [5]. This means that the signal for each product ion must be measured at its respective q^{max}_{prod}. For each product ion, its corresponding $\{[A^+]_0-[A^+]\}$ must also be measured at that same q^{max}_{prod}. That is, with reference to eq (4'), α must be determined by measuring $[C^+]$ and $\{[A^+]_0-[A^+]\}$ at the q^{max}_{prod} for C^+; with reference to eq (5'), β must be determined by measuring $[D^+]$ and $\{[A^+]_0-[A^+]\}$ at the q^{max}_{prod} for D^+; etc. This must be done to compensate for the differences in ion containment efficiencies within the Q2Q3 structure.

For example, consider the CAD of a parent ion of m/z 196 which fragments to progeny ions of m/z 15, m/z 42, and m/z 86 [5]. In this case α must be determined by measuring $[15^+]$ and $\{[196^+]_0-[196^+]\}$ at the q^{max}_{prod} for 15^+; β must be determined by measuring $[42^+]$ and $\{[196^+]_0-[196^+]\}$ at the q^{max}_{prod} for 42^+; etc. The reader may wish to consult reference [5] for a more detailed exposition.

In principle, if XQQ instruments were well behaved, all measurements could be made at the q^{max}_{prod} for the progeny ion of lowest mass (m/z 15 for the example above [5]). However, because of ion-optical imaging (focusing) problems within the Q2Q3 structure, one usually observes oscillations in the ion intensity as q_2 is varied [5]. Consequently, measurements of $[C^+]$, $[D^+]$, etc. and their respective $\{[A^+]_0-[A^+]\}$ must be made at the local maxima closest to the q^{max}_{prod} of each product ion.

3.2.2 Intrinsic Mass Discrimination (IMD) within Q3 The resolution controls for Q3 must be varied as necessary to compensate for the mass discrimination intrinsic to Q3 {cf. [2]: p. 100, p. 105 (fig. 5.9), and p. 143–144}.

3.2.3 The Kinetic Energy of Product Ions Entering Q3 It is now recognized that in the LAB frame of reference the translational energy of product ions E_{prod} is generally related to the collision energy of the projectile (reactant) ion E_{react} by:

$$E_{prod} \simeq (m_{prod}/m_{react})^n E_{react}, \quad (6)$$

where $n \simeq 1-2$ for CAD processes studied to date [8]. Hence, if $m_{prod}/m_{react} << 1$, low-mass daughters exiting Q2 will have low kinetic energies. Consequently, the Q3 rod offset (pole bias) must be set sufficiently low with respect to the Q2 rod offset so that no low-mass, low-energy product ions are denied entry to Q3 by the Q3 potential barrier. On the other hand, the Q3 potential barrier must be sufficiently high to provide adequate resolution within Q3 [8]. The reader may wish to consult references [7] and [8] for a more detailed exposition with reference to the selection of the appropriate Q3 rod offset.

4. Kinetics-Based Protocol for MS/MS Measurements

In this section we detail the generic protocol used to measure instrument-independent CAD spectra in XQQ instruments. The reader is referred to the caveats detailed in items 1–9 of the *Precautions* in Appendix 1.

(a) The protocol of Appendix 1 (for the NIST-EPA International Round Robin) must first be used to validate that any particular XQQ instrument can provide a dynamically-correct (i.e., instrument-independent) representation of ion-molecule reactions. If the instrument cannot pass the protocol (i.e., it cannot provide a dynamically-correct representation), one should not proceed any further until one has eliminated the ion-optical defect(s) so that the instrument can pass the protocol. If the instrument can provide a dynamically-correct representation, then the measurements for Part 1 of the round-robin protocol of Appendix 1 will provide an in situ calibration of the target thickness of the XQQ instrument.

(b) For all MS/MS measurements, one must use a gas target thickness within the single-collision regime [<2 cm-mtorr (<0.267 cm-Pa) for Ar]. For CAD, use an Ar gas target since it has been demonstrated [22] that the equivalent excitation energy (i.e., the equivalent internal energy imparted to a parent ion) is significantly less for a polyatomic target than it is for a monatomic target. However, one may also use other inert gas targets (He, Ne, Kr, or Xe) as necessitated by the collisional energy requirements since it has been demonstrated that the equivalent excitation energy is the same for the inert gases at any given center-of-mass energy E_{CM} [22]–[24] {$E_{CM} = E_{LAB}\ [m_2/(m_1+m_2)]$, where m_1 and m_2 are, respectively, the masses of the reactant ion and of the gas target}.

(c) One must use a *fixed* operating voltage for the ion detector (multiplier, Daly detector, etc.). The fixed voltage should provide the best compromise between the signal-to-noise ratio (S/N) of A^+ and the S/N of C^+, D^+, E^+, etc.

(d) One must make Conversion Gain measurements if an instrument uses analog current measurements. Conversion Gain is the ratio of the electron current output from an electron multiplier relative to the ion current input. The Conversion Gain measurements are used to correct for differences in mass-dependent detector response. If the instrument uses *true* ion pulse counting, Conversion Gain measurements are *not* needed [i.e., ignore instruction (d) and continue with instruction (e)].

Warning: Some instruments use analog current measurements, but report the ion intensities as equivalent ion count rates within their data systems. Such instruments still require Conversion Gain measurements.

Note: If possible, one should adjust the Conversion Gain of the ion detector so that one attains a mass-independent detector response. That is, so that the Conversion Gain is the same for a projectile ion and for its lowest-mass product ion (e.g., for CAD) or highest-mass product ion (e.g., for neutral gain reactions). This might be accomplished, for example, by adjusting the operating voltage of a high-voltage (e.g., 20–30 kV) conversion dynode which is used in conjunction with an electron multiplier. If it is not possible to attain a mass-independent detector response, then one must make corrections for difference in Conversion Gain for each parent ion and for each product ion.

To measure Conversion Gains, one may use a procedure analogous to that used for instructions 30–39 in Part 2 of the NIST-EPA round robin protocol in Appendix 1. However, to ensure that the most reliable correction factors are obtained, the mass-dependent Conversion Gain measurements would have to be made under actual operating conditions (viz., with the conversion dynode and electron multiplier at high voltages). This might be done by measuring the ion current striking the conversion dynode and relating it to the output current from the electron multiplier. One would have to demonstrate, however, that there is a one-to-one correspondence between the ion current input and the electron current output, independent of ion structure.

Note: For the rest of the instructions which follow, it is presumed that the ion signals correspond to a mass-independent detector response. That is, if necessary, the ion signals have been corrected for differences in Conversion Gain efficiency.

(e) Adjust the appropriate ion-optical elements (e.g., the Q1 rod offset for QQQ instruments) so that (i) $[B]_0 >> [A^+]_0$ and (ii) the energy spread of the projectile ions entering Q2 is minimized ($\leqslant$3 eV for 50% of the ions). (Refer to item 3 of the *Precautions* from the NIST-EPA round robin protocol in Appendix 1.) Measure the Q2 stopping curve in a manner analogous to that prescribed in instructions 8–10 of Part 1 of the NIST-EPA round-robin protocol in Appendix 1.

(f) From the optimum Q2 stopping curve measurements determine E_{50} (corresponds to the Q2 rod offset that stops 50% of the reactant ions). Then set the Q2 rod offset equal to $E_{50} - E_{LAB}$, where E_{LAB} is the requisite collision energy (in LAB coordinates).

(g) One must use only a "daughter-scan" mode. That is, Q1 is tuned to the peak position which corresponds to the maximum ion intensity at the m/z of the projectile ion while Q3 scans over the peak which corresponds to the m/z of a product ion. The q_2 must be referenced to q_1 (i.e., to q_{react}) rather than to q_3 (i.e., to q_{prod}). Use a scan window of ca. 4–10 amu so one can see the entire mass peak (baseline-to-baseline).

Note: To ensure consistent measurements for the duration of each experiment, make sure Q1 is staying tuned to the peak position for the projectile ion intensity; this can be done by varying the Q1 mass command to maximize the ion signal being viewed within the Q3 scan window. Use the same *fixed* operating voltage for the ion detector as was used for instruction 4 (c).

(h) One then adjusts iteratively the resolution parameters for Q3, and the Q3 rod offset as necessary to approximate $\alpha + \beta + \gamma + ... \simeq 1.0$ for the α, β, ..., etc. measured in concordance with the precepts detailed in sections 3.2.1–3.2.3. To optimize the precision of all measurements, ion signals should be measured in "back-to-back" units [cf. item 6 (iii) of the *Precautions* from the NIST-EPA round-robin protocol in Appendix 1]. For example, for a fixed [B]L measure:
$[C^+]$, $[A^+]$, and $[A^+]_0$ at the q_{prod}^{max} for C^+;
$[D^+]$, $[A^+]$, and $[A^+]_0$ at the q_{prod}^{max} for D^+; etc.

Note: One must make appropriate corrections for any background contributions to $[C^+]$, $[D^+]$, etc. which may be observed in the absence of added target gas. Such background contributions can arise from decompositions of A^+ (to produce C^+, D^+, etc. via CAD or RIF [9]) occurring between the rear of Q1 and the front of Q3. Such background CAD or RIF may be induced by the interaction of A^+ with plumes of gas emanating from the ion source.

(i) In practice, instructions (b)–(h) provide IMD-free and RIMD-free estimates for the branching ratios of fragment ions, except for very minor fragment ions adjacent to major ions. The resolution is not adequate for obtaining dynamically-correct estimates for the branching ratios of very minor fragment ions adjacent to major ions. Consequently, the resolution must be increased for each group of ions which contains a minor ion adjaent to a major ion, and complementary measurements must be made for the branching ratios of minor fragment ions within each group. Each group contains only fragment ions which are in close proximity (e.g., m/z 13–15), so that the measurements for each ion in the group are still IMD-free and RIMD-free within that group. To relate these individual group measurements to the overall CAD spectrum [viz., to the entire range of masses from the m/z of the reactant (parent) ion down to the m/z of the lowest-mass product ion], the measurements for each group must be referenced to the IMD-free and RIMD-free estimate for the branching ratio of a major fragment ion within that group. For example, for $E_{CM} \simeq 2-40$ eV, the CAD of $C_2H_3O^+$ (m/z 43) from biacetyl pro-

duces fragment ions at the following m/z: 13, 14, 15, 26, 27, 28, 29. The fragment ions at m/z 13 and 14 are minor compared to the major fragment ion at m/z 15 (refer to table 1). Therefore, m/z 13–15 are measured under well-resolved conditions and referenced to the IMD-free and RIMD-free estimate for the branching ratio of the fragment ion at m/z 15. Similarly, the fragment ions at m/z 27 and 28 are referenced to the fragment ions at m/z 26 and/or 29.

(j) Repeat (b)–(i) as necessary to accomplish $\propto+\beta+\gamma+...\simeq 1.0\pm 0.1$ for each E_{CM}, as necessitated by the reaction dynamics.

5. Proposed Format for MS/MS Database

Table 1 shows a typical CAD spectrum (measured with the protocol of sec. 4 [16]) in the format proposed for presentation of CBRIS.

5.1 Advantages

The advantages of this CBRIS database format are:

(a) The partial cross sections $\propto\sigma$, $\beta\sigma$, etc. can characterize both known and unknown species (so long as the unknown species contain ionic substructures for which the CAD cross sections and product identities are known). Therefore, it may be possible to assign the structure of an *unknown* species on the basis of the absolute cross sections σ_{ij}, σ_{jk}, etc. for the CAD of *known* ionic substructures i, j, k, etc. That is, this proposed use of CBRIS in MS/MS is analogous to the use of group frequencies in infrared spectroscopy.

(b) Characterization of an unknown compound by using CBRIS does not require that the compound be in the CBRIS database. By contrast, to characterize an unknown by spectral matching within a "library", the compound must usually be in the library. In this regard, development of a *database* of CBRIS for all substructures (or a subset thereof) would be very much more tractable than the development of a *library* of CAD spectra for all the source compounds that contain all the substructures (or a subset thereof). For example, consider the simplistic analogy where compounds correspond to words, and substructures correspond to letters: more than 500,000 words can be composed with only 26 letters of the alphabet.

(c) The format is compatible with its use in expert systems. This should facilitate rapid real-time analysis of unknowns within computer-controlled field instruments.

(d) End users are involved directly in its evolution by using critically evaluated cross sections already in the database and by submitting new cross sections for inclusion in the database.

6. Conclusions

A kinetics-based measurement protocol can provide accuracy and precision for CAD measurements within XQQ tandem mass spectrometers. This protocol can be used to develop a dynamically-correct (i.e., instrument-independent) MS/MS database (or library) for XQQ instruments.

7. Acknowledgments

I gratefully acknowledge the funding of this work, in part, by the U.S. Environmental Protection Agency [the Emergency Response Team (ERT) and the Atmospheric Research and Exposure Assessment Laboratory (AREAL)] under Interagency Agreements IAG #DW-13932911 and DW-13933643.

Volume 94, Number 5, September–October 1989
Journal of Research of the National Institute of Standards and Technology

Appendix 1. NIST-EPA Round Robin for XQQ Instruments (QQQ, BEQQ, etc.): A Test Protocol to Assess Which Instrument Designs Provide Instrument-Independent (Dynamically-Correct) Performance

Note: This appendix is the full text of the actual document which was sent to, and was used by, the participants in the NIST-EPA International Round Robin. The round-robin results have been published elsewhere [21]. *This document may be photocopied. Prospective participants may submit test data to the author anytime for this ongoing evaluation project.*

This round robin is being coordinated by Dr. Richard I. Martinez of the U.S. National Institute of Standards and Technology (NIST). It is sponsored by the Environmental Monitoring Systems Laboratory (EMSL) of the U.S. Environmental Protection Agency (EPA).

Address Inquiries/Comments to: Richard I. Martinez, A260 Chemistry Bldg.
NIST, Gaithersburg, MD 20899 USA
Telephone: (301) 975-2516
FAX: (301) 975-2128

Objective

To assess which XQQ instrument designs can be used to generate a generic, instrument-independent MS/MS database. To do so, an XQQ instrument (QQQ, BEQQ, etc.) must provide a dynamically-correct (instrument-independent) representation of any ion-neutral interaction (e.g., CAD, etc.) studied within its Q2Q3 structure. The prerequisites for obtaining dynamically-correct branching ratios within XQQ instruments have been detailed in reference [9].

Data Analysis

To ensure consistency, all data will be analyzed by the round-robin coordinator. The participants will provide only "raw data" on the forms provided with the test protocol. To perform the analysis, the raw data will have to include information about such technical specifications as field radius, rf frequency, etc. Please submit one completed copy of the *Questionnaire* for each XQQ instrument included in the round robin.

Confidentiality

All information provided by participants will be confidential. No proprietary information will be divulged. No participant or instrument manufacturer will be identified (the data files will be encrypted with code letters, numbers, and symbols known only to the round-robin coordinator). All test results will be discussed only in generic terms.

Summary of Test Protocol

The test protocol is based on (i) the concepts detailed in reference [9], and (ii) the use of the ion-neutral reaction kinetics of references [12] and [14].

The following is a synopsis of the two major components of the test protocol. The nomenclature used herein is defined in references [9], [12], and [14].

Part 1

Purpose

(i) To determine if the reaction kinetics are well controlled (i.e., no back reactions, no scattering losses, minimal fringing fields, no mass discrimination, well-defined gas target, etc.) within each XQQ instrument. The symmetric charge transfer reaction $^{36}Ar^+ + {}^{40}Ar \rightarrow {}^{36}Ar + {}^{40}Ar^+$ is used (see reference [12]). In this case there is no reaction-induced mass discrimination (defined in reference [9]).

(ii) To calibrate the response of the pressure sensor closest to the participant's collision region in terms of the effective target thickness $[Ar]L_{eff}$ within the collision region (L_{eff} is the effective pathlength of the complex oscillatory trajectory traversed by a projectile ion through the CAD target gas within Q2). This is done to ensure all participants use the same effective target thickness measurements.

Glossary

Here we describe some terms used below.

NISTCALPLOT A calibration curve of ln Y (=ln W) vs effective target thickness $[Ar]L_{eff}$. NISTCALPLOT (fig. 1) is included below for use with the test protocol.

P/XQQ The nominal pressure indicated by some sensor located closest to the participant's collision region (see *Precaution* 8).

ARLEFF/LNY The target thickness $[Ar]L_{eff}$ which is derived from NISTCALPLOT for a corresponding ln Y value measured by a participant for a given P/XQQ.

ARLEFF/LNW The target thickness $[Ar]L_{eff}$ which is derived from NISTCALPLOT for a corresponding ln W value measured by a participant for a given P/XQQ.

XQQCALPLOT A graph containing a plot of ARLEFF/LNY vs P/XQQ and a plot of ARLEFF/LNW vs P/XQQ.

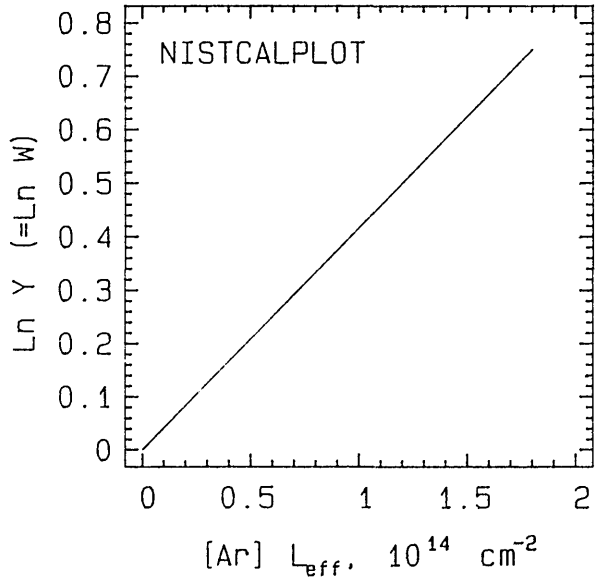

Figure 1. Calibration curve of ln Y (=ln W) vs effective target thickness $[Ar]L_{eff}$.

Method

Using several different pressures (P/XQQ) of Ar target gas, each participant measures ln Y *and* ln W for the reaction $^{36}Ar^+ + {}^{40}Ar \rightarrow {}^{36}Ar + {}^{40}Ar^+$. NISTCALPLOT is then used to convert the participant's ln Y and ln W measurements to the corresponding target thicknesses ARLEFF/LNY and ARLEFF/LNW, respectively. These data are then used to prepare the calibration graph XQQCALPLOT. If the kinetics are well controlled within the participant's XQQ instrument, then the two plots of ARLEFF/LNY vs P/XQQ and ARLEFF/LNW vs P/XQQ should be superimposable.

Part 2

Purpose

To assess how well one can correct for reaction-induced mass discrimination and for strong ion-optical imaging (focusing) problems within the Q2Q3 structure (i.e., how well one can control the key MS/MS parameters in different XQQ instrument designs) (see reference [9] for further information).

Method

Each participant measures ln *Y and* ln *W* for the reaction $N_2^+ + SF_6 \rightarrow N_2 + SF_5^+$ as a function of the pressure P/XQQ of the SF_6 gas target (cf. reference [14]).

Data Format

Different types of data are requested within the test protocol. Most of the test data to be provided by the participants will consist of "filling-in-the-blanks" in the spaces provided with the test protocol.

For laboratories with more than one XQQ instrument participating in the round-robin test, please submit a separate set of data for each XQQ instrument (use photocopies of this test protocol document to record each separate set of data).

Precautions

1. Manual vs Automated Control

Some very sophisticated XQQ systems have automated ("intelligent") self-tuning capabilities (e.g., mass calibration, etc.), automated instrument control (e.g., "programmed ion optics", MS/MS mass scan modes, etc.) and automated data acquisition, etc.

To provide the best possible assessment of instrument *Hardware* design (without obfuscation by software artifacts), and to ensure consistency among the data submitted, participants must *not* use any of the automated capabilities.

Instrument control and data acquisition should be as close to "manual" control as is possible with your instrument. You may use a "hybrid" control system wherein you are "manually" controlling the parameters [e.g., programmable "soft-knobs" (EXTREL[1]) or "tuning tables" (Finnigan TSQ70) are used to vary the dc voltage which is being applied to a lens via a digital-to-analog converter (DAC)]. However, use only a single "tuning table" with "flat" (constant) parameter settings; don't use "programmed ion optics". Please mark the top of the first page of the submitted data with the following label: *Manual Instrument Control and Data Acquisition.*

However, for any one XQQ instrument being tested, participants are welcome to submit a *second* set of data to assess possible artifacts in the instrument control and data acquisition software. Please mark the top of the first page of the submitted data with the following label: *Automated Instrument Control and Data Acquisition.*

If your system has only automated capabilities (i.e., there is absolutely no way that it can be made to function in a manual or hybrid mode of operation for instrument control and data acquisition), please mark the top of the first page of the submitted data with the following label: *Non-Manual Instrument Control and Data Acquisition.*

[1] Certain commercial equipment, instruments, and materials are identified in this paper in order to adequately specify the experimental procedure. In no case does such identification imply recommendation or endorsement by the National Institute of Standards and Technology, nor does it imply that the material, instruments, or equipment identified is necessarily the best available for the purpose.

2. Actual Voltage Measurements

The actual voltages of all essential ion-optical elements [rod offset (pole bias) of Q1, Q2, Q3; lens potentials; etc.] must be measured with a voltmeter at the appropriate measurement test points closest to each ion-optical element. Consult the manufacturer for the location of each test point and the method of measurement that you should use to ensure correct values (e.g., to measure actual rod offsets, you may have to disconnect the inputs for mass command and/or resolution control and/or ΔM control). Please make actual voltage measurements to validate any voltage information provided by a computer system via an analog-to-digital converter (ADC).

3. Q1 Rod Offset and Projectile Energy Distribution

To be kinetically meaningful, participants must ensure:

(a) that $[B]_0 >> 100[A^+]_0$ (in molecules cm^{-3} within Q2; ion intensity data are converted to the approximate ion concentrations with reference to the defining aperture which provides entry into Q2),
(b) that the measured reactivity can be attributed to a well-characterized state of the projectile ion A^+, and
(c) that the translational energy distribution of the projectile ion entering Q2 is reasonably narrow (cf. Q2 stopping curve data in references [12] and [14]). [Unfortunately, narrowing the energy distribution of the projectile ion can produce ion-optical imaging (focusing) problems within Q2 if the XQQ instrument has restrictive interquadrupole apertures (see reference [9]).]

For QQQ instruments, tasks (a)–(c) can be accomplished by over-resolving Q1 (i.e., increasing the resolution of Q1 to produce a sharp, narrow peak) and by raising the Q1 rod offset close to the ion source potential. The effect of these actions is to: (i) discard a large fraction (>90%) of A^+, (ii) delay the transit of A^+ through Q1 (this provides sufficient time for excited electronic states of the N_2^+ used for *Part 2* to be quenched by radiative transitions prior to their entry into Q2), and (iii) reduce the energy spread of the ions exiting Q1 by cutting out low-energy ions. Unfortunately, rf-pickup within each quadrupole mass filter tends to broaden the energy distribution of the projectile ion as it traverses Q1, Q2, and Q3. Therefore, a high-energy tail is usually observed.

4. Q3 Rod Offset

To achieve $\ln W = \ln Y$, one must have very high ion-collection-efficiency ($\simeq$100%). Consequently, the Q3 rod offset must be biased very *negatively* with respect to the Q2 rod offset to draw ions out of Q2. This will result in very broad, poorly resolved mass peaks (reference [8] shows examples of how the Q3 rod offset affects peak shapes). Throughout each *Part* of the test protocol, you must keep the Q3 rod offset biased as negatively as necessary so that $[C^+] \simeq [A^+]_0 - [A^+]$.

5. Tuning q_2

The rf amplitude of Q1, Q2, and Q3 is characterized here by the Mathieu parameters q_1, q_2, and q_3, respectively (for further information, see references [2]–[5]). Some instruments have a separate rf/dc generator (quadrupole controller/power supply) for each of the three quadrupole rod assemblies (Q1, Q2, and Q3); some do not. Some can reference q_2 to q_3 *and/or* to q_1 (i.e., one can vary q_2/q_1 or q_2/q_3 from 0–1; in some instruments the ratio is fixed at $q_2/q_1 = 0.5$ or $q_2/q_3 = 0.5$). Some instruments reference q_2 to the ion transmission cut-off which occurs at $q_2 \simeq 0.908$ [this latter mode of tuning is somewhat risky; the rf-pickup within Q2 can make it difficult to distinguish the true cut-off at $q_2 \simeq 0.908$ from the small, but significant contribution of ions in the high energy tail which are transmitted through Q2Q3 even though the nominal (apparent) value is $q_2 > 0.908$].

In general, tune q_2 by following the recommendations of the manufacturer of your XQQ instrument (please complete the questionnaire regarding modes of operation for your XQQ instrument). However, to ensure experimental consistency among participants, please validate your q_2 values relative to q_1 and/or q_3 (i.e., remember that whenever Q1 or Q3 are operated in a well-resolved mode and are tuned to any m/z, then the mass peak position corresponds to $q_1 \simeq 0.706$ or $q_3 \simeq 0.706$ for that m/z).

One can accomplish the validation of q_2 values with a simple potentiometer divider circuit if the instrument can be operated in a manual or hybrid mode. For example, in some instruments a *Mass Command* input dc voltage (typically 0–10 V) is used to control the rf amplitude of a quadrupole mass filter. This 0–10 V is usually supplied by a DAC which may be controlled by a computer via a programmable soft-knob. Here we use MC1, MC2, and MC3 to designate, respectively, the 0–10 V *Mass Command* input voltages for Q1, Q2, and Q3. Then the divider potentiometer can be used to vary q_2/q_1 ($\simeq$MC2/MC1) or q_2/q_3 ($\simeq$MC2/MC3). Consult your manufacturer for the location of the inputs analogous to MC1, MC2, and MC3.

If the manufacturer asserts there is absolutely no possible way to vary q_2 within your instrument (i.e., one cannot vary q_2/q_1 or q_2/q_3), please indicate how q_2 is controlled by the manufacturer (i.e., does the manufacturer use a fixed value of q_2/q_1 or $q_2/q_3 \simeq 0.5$, or ?). Also, please mark the top of the first page of the submitted data with the following label: q_2 *Not Varied.*

6. Acquisition of Ion Intensity Data

(i) Mode of Operation

Use only a "daughter-scan" mode [i.e., q_2 referenced to q_3; Q1 tuned to the peak position which corresponds to the maximum ion intensity at the m/z of the projectile ion; Q3 scanning over the peak which corresponds to the m/z of the product ion (use a scan window of ca. 4–10 amu) so you can see the entire mass peak (baseline-to-baseline)].

Note: To ensure consistent measurements for the duration of each experiment, make sure Q1 is staying tuned to the peak position for the projectile ion intensity; this can be done by varying the Q1 mass command to maximize the ion signal being viewed within the Q3 scan window.

(ii) Signal and Background Measurements

For the reasons discussed in 1 above, all ion signal intensities must be acquired *manually*. To do so, you must use a display which shows the *complete* mass spectral peak shape for a single mass peak (i.e., baseline-to-baseline display of ion intensity vs m/z for a single mass peak). For this, you can use either an external oscilloscope connected to the output of your detector chain, or whatever mass spectral display your system provides on its CRT.

For each mass peak, use arbitrary units (e.g., CRT divisions) to measure the ion intensity at the peak. However, report the ion intensities in relative units by making appropriate corrections for differences in amplifier gain, scope attenuation, etc. [e.g., an ion intensity of *1.00 relative units* could correspond to (a) 1 CRT division with an amplifier gain of $\times 1$ and a scope attenuation of $\times 1$, etc. or (b) 10 CRT divisions with an amplifier gain of $\times 100$ and a scope attenuation of $\times 10$].

For the measurement of *background* alone, the ion intensity is measured at the mass peak position in the absence of the ion of interest. For the measurement of *signal + background*, the ion intensity is measured at the mass peak position in the presence of the ion of interest.

Note: Please follow the following guidelines to ensure the ion intensity measurements are kinetically meaningful, and to minimize long-term variations in gas flows, detector response, etc. Here source gas refers to the gas introduced into the ion source, and target gas refers to the gas introduced into Q2.

(a) Before making any ion intensity measurements in Part 1 or Part 2, allow sufficient "warm-up" time to ensure all instrumental components, ion source, gas flows, etc. have stabilized.

(b) Leave *everything* (source gas, ionizer filament, etc.) turned on at all times for the duration of all measurements in any one Part (the target gas is the only thing that should be turned on and off during the measurements).

(c) If possible, use a high-quality toggle valve or solenoid shut-off valve to turn the target gas on/off. (The shut-off valve should be located between the Q2 collision region and a high-precision needle valve). Thus, the target gas flow can be reset reproducibly to any given P/XQQ by presetting the needle valve. This will help to ensure high-accuracy "back-to-back" units for ln Y/ln W measurements.

(d) To make measurements of the *background* intensity at any m/z, block the Projectile Ion Beam (PIB). To do so, raise to a high positive voltage the potential of any ion-optical element (e.g., the rod offset of Q1 or Q2).

The following abbreviations are used throughout the protocol:
PIBOFF=Projectile Ion Beam OFF (projectile ion beam blocked; no ions reach the detector)
PIBON =Projectile Ion Beam ON (projectile ion beam unblocked; ions enter Q2)
TGOFF =Target Gas OFF (not flowing into Q2)
TGON =Target Gas ON (flowing into Q2)

(iii) ln Y and ln W Measurements

All ln Y and ln W data should be collected in *back-to-back units* to minimize long-term variations in gas flows, detector response, etc. For example, with reference to equations (1) and (2), one back-to-back unit would consist of items (a)–(g) below. Here q_{react}^{max} and q_{prod}^{max} represent, respectively, the values of q_2 which correspond to the maximum ion transmission through Q2Q3 for the reactant (projectile) ion A^+ and for the C^+ product ion. Note that q_{react}^{max} and q_{prod}^{max} must be known prior to making the ln Y and ln W measurements.
(a) tune q_2 to q_{react}^{max} for A^+.
(b) PIBOFF/TGOFF: measure background signal at $m/z(A^+)$.
(c) PIBON/TGOFF: measure $[A^+]_0$ at $m/z(A^+)$.
(d) PIBON/TGOFF: tune q_2 to q_{prod}^{max} for C^+; measure background signal at $m/z(C^+)$.
(e) PIBON/TGON: measure $[C^+]$ at $m/z(C^+)$; tune q_2 to q_{react}^{max}; measure $[A^+]$ at $m/z(A^+)$.
(f) repeat (c).
(g) repeat (b).

(iv) Detector Conversion Gain

Use a *fixed* operating voltage for your ion detector (multiplier, Daly detector, etc.). The fixed voltage used for measurements within *Part 1* can differ from the fixed voltage used for *Part 2*. But you must use the same fixed voltage for all back-to-back units within any one Part. For each Part, the fixed voltage should provide the best compromise between the S/N of A^+ and the S/N of C^+.

7. Target Gas Purity

The purity of the Ar and SF_6 target gases should be >99.99%.

8. P/XQQ Measurements

There are only two requirements for P/XQQ measurements: (1) that the sensor being used must provide a *reproducible, single-valued* response for any given target gas pressure of Ar, and (2) that you know the relative sensitivity of the sensor (i.e., its response factor) for SF_6 relative to Ar. For example, some instruments use a mass flowmeter to measure the flow rate of the target gas into the collision region. You could use the flowmeter response if you know its response factor for SF_6 and for Ar.

9. High-Vacuum Materials

No plastic tubing (teflon, etc.) should be used to introduce the high-purity target gas into the collision region within Q2. The target gas should flow only through materials normally used in high-vacuum applications (bellows valves, etc.). This will ensure that the ln Y and ln W measurements are not complicated by reactions of the projectile ion with impurities inadvertently admixed with the target gas. If you do have plastic parts in contact with the target gas, and can't substitute high-vacuum materials for the duration of this test, please mark the top of the first page of the submitted data with the following label: *Plastic Tubing Used*.

Test Protocol

Note: Before proceeding with the test protocol, please read the *Precautions* above, familiarize yourself with all the steps of the test protocol, and refer to references [9], [12], and [14] as necessary. To ensure consistency among participants, all tuning procedures and measurements must be carried out in accord with the *Precautions*. Please be sure to observe *Precaution 4*. If you have any questions, please call the round-robin coordinator.

Note: Record all ion intensities in *relative units (Precaution 6.)* in the spaces provided with each instruction.

Part 1. $^{36}Ar^+ + {}^{40}Ar \rightarrow {}^{36}Ar + {}^{40}Ar^+$

Note: After you find the tuning conditions that achieve ln $Y \simeq$ ln W (i.e., $[^{40}Ar^+] \simeq [^{36}Ar^+]_0 - [^{36}Ar^+]$), the same parameter settings (lens potentials, etc.) must be used for ln W measurements as are used for ln Y measurements.

Note: For instructions 1–7 below, maintain a constant difference of ca. 40 eV between the nominal Ion Source Potential (ISP) and the Q2 Rod Offset (Q2RO); i.e., ISP-Q2RO$\simeq$*40 eV*.

Warning: If your instrument can only achieve a nominal collision energy which is *less than* 40 eV (LAB), please indicate here your maximum achievable collision energy.

_____ eV (LAB)

If you *cannot* achieve 40 eV (LAB), then use your maximum achievable collision energy in lieu of 40 eV for all measurements in Part 1 and Part 2.

Initial Tuning:

1. PIBON/TGOFF: Set Q1 and Q3 at the mass peak position for $^{36}Ar^+$. Measure the ion intensity at the mass peak position ($\simeq[^{36}Ar^+]_0$).
2. Repeat 1., but with PIBOFF/TGOFF to measure the corresponding background intensity.
3. PIBON/TGON: Add sufficient Ar target gas so the ion intensity $[^{36}Ar^+]$ becomes ca. 0.5 $[^{36}Ar^+]_0$.
4. Repeat 3., but with PIBOFF/TGON to measure the corresponding background intensity.
5. PIBON/TGON: Set Q1 at the mass peak position for $^{36}Ar^+$ and Q3 at the mass peak position for $^{40}Ar^+$. Measure the ion intensity at the mass peak position for $^{40}Ar^+$ ($\simeq[^{40}Ar^+]$).
6. Vary all the ion-optical elements of your instrument (q_2, lens potentials, rod offsets, resolution and ΔM control, etc.) as necessary to maximize $[^{40}Ar^+]$ and to roughly approximate $[^{40}Ar^+] \simeq [^{36}Ar^+]_0 - [^{36}Ar^+]$.
7. Repeat 1–6 through as many iterations as necessary to achieve $[^{40}Ar^+] \simeq [^{36}Ar^+]_0 - [^{36}Ar^+]$.

Q2 Stopping Curve (cf. *Precaution 3*):

8. PIBON/TGOFF: Set Q1 and Q3 at the mass peak position for $^{40}Ar^+$. Measure $[^{40}Ar^+]_0$ as a function of the Q2 rod offset (Q2RO) to generate a Q2 stopping curve. Vary Q2RO over a range of potentials from ca. 10 eV below the nominal ion source potential to just above the nominal ion source potential where 99% of the projectile ions are stopped. For each Q2RO used, retune q_2 to q_{react}^{max} before measuring each $[^{40}Ar^+]_0$ for the corresponding Q2RO. Plot $[^{40}Ar^+]_0$ vs Q2RO.
9. If your Q2 stopping curve (energy distribution) doesn't approximate that of reference [12] (viz. a sharp cutoff), raise the Q1 rod offset closer to the ion source potential. Then repeat 1–7, as necessary, to ensure that the tuning of the ion-optical elements has maintained $[^{40}Ar^+] \simeq [^{36}Ar^+]_0 - [^{36}Ar^+]$. Then repeat 8 (and 9 if necessary).
10. For your final Q2 stopping curve, enter the values of $[^{40}Ar^+]_0$ vs the Q2 rod offset (Q2RO) in the spaces provided, and submit a hardcopy of the corresponding plot.

$[^{40}Ar^+]_0$	_____	_____	_____	_____	_____	_____	_____	_____
Q2R0, V	_____	_____	_____	_____	_____	_____	_____	_____
$[^{40}Ar^+]_0$	_____	_____	_____	_____	_____	_____	_____	_____
Q2R0, V	_____	_____	_____	_____	_____	_____	_____	____

$[^{40}Ar^+]_0$	_____	_____	_____	_____	_____	_____	_____	_____
Q2R0, V	_____	_____	_____	_____	_____	_____	_____	_____

Please submit a record of the settings of all your ion-optical elements (lenses, rod offsets, etc.) used to accomplish 10. Also, please submit a copy of a simplified schematic diagram (layout) showing the ion-optical components of your instrument from the ion source through the detector. Please label each ion-optical element so we can identify the settings with the schematic layout.

Note: Use the final Q2 stopping curve developed in instruction 10 to determine E_{50} (≡the Q2 rod offset that stops 50% of the projectile ions). For instructions 11–31 below, set the Q2 rod offset= (E_{50}−40) eV and set *all* the other ion-optical elements to the same values as were used for the final Q2 stopping curve of instruction 10.

Interference of $^{40}Ar^+$ at *m/z* 36 and of $^{36}Ar^+$ at *m/z* 40:

11. PIBON/TGOFF: Set Q1 at the mass peak position for $^{36}Ar^+$ and Q3 at the mass peak position for $^{36}Ar^+$ [*Precaution* 6 (i)]. Measure and record the intensity at the mass peak position for $^{36}Ar^+$. _____
12. Repeat 11, but with PIBOFF/TGOFF to measure the corresponding background intensity. _____
13. PIBON/TGOFF: Set Q1 at the mass peak position for $^{36}Ar^+$ and Q3 at the mass peak position for $^{40}Ar^+$. Measure and record the intensity at the mass peak position for $^{40}Ar^+$. _____
14. Repeat 13, but with PIBOFF/TGOFF to measure the corresponding background intensity. _____
15. PIBON/TGOFF: Set Q1 at the mass peak position for $^{40}Ar^+$ and Q3 at the mass peak position for $^{40}Ar^+$. Measure and record the intensity at the mass peak position for $^{40}Ar^+$. _____
16. Repeat 15, but with PIBOFF/TGOFF to measure the corresponding background intensity. _____
17. PIBON/TGOFF: Set Q1 at the mass peak position for $^{40}Ar^+$ and Q3 at the mass peak position for $^{36}Ar^+$. Measure and record the intensity at the mass peak position for $^{36}Ar^+$. _____
18. Repeat 17, but with PIBOFF/TGOFF to measure the corresponding background intensity. _____

ln *Y* and ln *W* Measurements:

All ln *Y*/ln *W* measurements within this Part 1 should be done at the same time (cf. *Precaution* 6). Record P/XQQ, ln *Y*, ln *W*, ARLEFF/LNY, and ARLEFF/LNW in the spaces provided. Please observe *Precaution* 8..

For $[^{36}Ar^+]/[^{36}Ar^+]_0 \simeq 0.5$:

19. PIBON/TGOFF: Set Q1 and Q3 at the mass peak position for $^{36}Ar^+$. Measure the ion intensity at the mass peak position ($\simeq[^{36}Ar^+]_0$). _____
20. Repeat 19, but with PIBOFF/TGOFF to measure the corresponding background intensity. _____
21. PIBON/TGON: Add sufficient Ar target gas so the ion intensity becomes $[^{36}Ar^+] \simeq 0.5\ [^{36}Ar^+]_0$. Measure the ion intensity at the mass peak position ($\simeq[^{36}Ar^+]$). _____
22. Repeat 21, but with PIBOFF/TGON to measure the corresponding background intensity. _____
23. PIBON/TGON: Set Q1 at the mass peak position for $^{36}Ar^+$ and Q3 at the mass peak position for $^{40}Ar^+$. Measure the ion intensity at the mass peak position for $^{40}Ar^+$ ($\simeq[^{40}Ar^+]$). _____

P/XQQ=_____ ln *Y*=_____ ln *W*=_____
ARLEFF/LNY=_____ ARLEFF/LNW=_____

24. Repeat 19–23, but with sufficient Ar target gas so that $[^{36}Ar^+]/[^{36}Ar^+]_0 \simeq 0.8$. Record your measurements in the spaces provided for the corresponding instructions.

"19."_____ "20."_____ "21."_____ "22."_____ "23."_____
P/XQQ=_____ ln *Y*=_____ ln *W*=_____
ARLEFF/LNY=_____ ARLEFF/LNW=_____

25. Repeat 19–23, but with sufficient Ar target gas so that $[^{36}Ar^+]/[^{36}Ar^+]_0 \simeq 0.6$. Record your measurements in the spaces provided for the corresponding instructions.

"19."_____ "20."_____ "21."_____ "22."_____ "23."_____
P/XQQ=_____ ln Y=_____ ln W=_____
ARLEFF/LNY=_____ ARLEFF/LNW=_____

26. Repeat 19–23, but with sufficient Ar target gas so that $[^{36}Ar^+]/[^{36}Ar^+]_0 \simeq 0.9$. Record your measurements in the spaces provided for the corresponding instructions.

"19."_____ "20."_____ "21."_____ "22."_____ "23."_____
P/XQQ=_____ ln Y=_____ ln W=_____
ARLEFF/LNY=_____ ARLEFF/LNW=_____

27. Repeat 19–23, but with sufficient Ar target gas so that $[^{36}Ar^+]/[^{36}Ar^+]_0 \simeq 0.7$. Record your measurements in the spaces provided for the corresponding instructions.

"19."_____ "20."_____ "21."_____ "22."_____ "23."_____
P/XQQ=_____ ln Y=_____ ln W=_____
ARLEFF/LNY=_____ ARLEFF/LNW=_____

28. Repeat 19–23 for $[^{36}Ar^+]/[^{36}Ar^+]_0 \simeq 0.5$:

"19."_____ "20."_____ "21."_____ "22."_____ "23."_____
P/XQQ=_____ ln Y=_____ ln W=_____
ARLEFF/LNY=_____ ARLEFF/LNW=_____

29. PIBON/TGOFF: Set Q1 and Q3 at the mass peak position for $^{36}Ar^+$. Measure the ion intensity at the mass peak position ($\simeq[^{36}Ar^+]_0$). _____
30. Repeat 29, but with PIBOFF/TGOFF to measure the corresponding background intensity. _____
31. Generate XQQCALPLOT by plotting ARLEFF/LNY vs P/XQQ and ARLEFF/LNW vs P/XQQ on the same graph. Submit a hardcopy of your XQQCALPLOT graph.

Note: If the two plots are not superimposable [i.e., same slope and intercept (to within ±10%)], your instrument HARDWARE does not have a dynamically-correct design (cf. reference [9]). Nonetheless, please proceed with Part 2 to assess other aspects of your instrument design.

Part 2. $N_2^+ + SF_6 \rightarrow N_2 + SF_5^+$

Note: In Part 2, you will be tuning you instrument to achieve $[SF_5^+] \simeq [N_2^+]_0 - [N_2^+]$. However, your detector may suffer significant differences in absolute response for SF_5^+ vs N_2^+ [i.e., the Conversion Gain CG_{127} for SF_5^+ (m/z 127) may differ substantially from the conversion gain CG_{28} for N_2^+ (m/z 28)]. You will, therefore, determine CG_{127}/CG_{28} at the end of Part 2. In the meantime, observe *Precaution* 6 (iv), and maximize $[SF_5^+]$ to approximate as best you can $[SF_5^+] \simeq [N_2^+]_0 - [N_2^+]$. For example, if $CG_{127}/CG_{28} \simeq 0.9$, you may find the best you can do is $[SF_5^+] \simeq 0.8\{[N_2^+]_0 - [N_2^+]\}$.

Note: Please observe *Precaution* 8. For the sensor you are using to make P/XQQ measurements, record here the type of sensor (Bayard-Alpert Ion Gauge, mass flowmeter, etc.) and its relative sensitivity (i.e., the response factor) for SF_6 relative to Ar.
Type of sensor_____ Response Factor (SF_6/Ar)_____

Note: For instructions 1–7 below, maintain a constant difference of ca. 40 eV between the nominal Ion Source Potential (ISP) and the Q2 Rod Offset (Q2RO); i.e., ISP-02RO≃40 eV.

Warning: If your instrument can only achieve a nominal collision energy which is *less than* 40 eV (LAB), then use your maximum achievable collision energy in lieu of 40 eV, as you did for Part 1.

Initial Tuning:

1. PIBON/TGOFF: Set Q1 and Q3 at the mass peak position for N_2^+ with $q_2=q_{react}^{max}$. Measure the ion intensity at the mass peak position ($\simeq[N_2^+]_0$).
2. Repeat 1, but with PIBOFF/TGOFF to measure the corresponding background intensity.
3. PIBON/TGON: Add sufficient SF_6 target gas so the ion intensity $[N_2^+]$ becomes ca. 0.6 $[N_2^+]_0$.
4. Repeat 3, but with PIBOFF/TGON to measure the corresponding background intensity.
5. PIBON/TGON: Set Q1 at the mass peak position for N_2^+ and Q3 at the mass peak position for SF_5^+ (m/z 127). Measure the ion intensity at the mass peak position for SF_5^+ ($\simeq[SF_5^+]$).
6. Vary all the ion-optical elements of your instrument ($q_2=q_{prod}^{max}$, lens potentials, rod offsets, resolution and ΔM control, etc.) as necessary to maximize $[SF_5^+]$ and to roughly approximate $[SF_5^+]\simeq[N_2^+]_0-[N_2^+]$.
7. Repeat 1–6 through as many iterations as necessary to optimize $[SF_5^+]\simeq[N_2^+]_0-[N_2^+]$.

Q2 Stopping Curve (cf. *Precaution* 3):

8. PIBON/TGOFF: Set Q1 and Q3 at the mass peak position for N_2^+. Measure $[N_2^+]_0$ as a function of the Q2 rod offset (Q2RO) to generate a Q2 stopping curve. Vary Q2RO over a range of potentials from ca. 10 eV below the nominal ion source potential to just above the nominal ion source potential where 99% of the projectile ions are stopped. For each Q2RO used, retune q_2 to q_{react}^{max} before measuring each $[N_2^+]_0$ for the corresponding Q2RO. Plot $[N_2^+]_0$ vs Q2RO.
9. If your Q2 stopping curve (energy distribution) doesn't approximate that of reference [14], raise the Q1 rod offset closer to the ion source potential. Then repeat 1–7, as necessary, to ensure that the tuning of the ion-optical elements has maintained $[SF_5^+]\simeq[N_2^+]_0-[N_2^+]$. Then repeat 8 (and 9 if necessary).
10. For your final Q2 stopping curve, enter the values of $[N_2^+]_0$ vs the Q2 rod offset (Q2RO) in the spaces provided, and submit a hardcopy of the corresponding plot.

$[N_2^+]_0$	_____	_____	_____	_____	_____	_____	_____	_____
Q2R0, V	_____	_____	_____	_____	_____	_____	_____	_____
$[N_2^+]_0$	_____	_____	_____	_____	_____	_____	_____	_____
Q2R0, V	_____	_____	_____	_____	_____	_____	_____	_____
$[N_2^+]_0$	_____	_____	_____	_____	_____	_____	_____	_____
Q2R0, V	_____	_____	_____	_____	_____	_____	_____	_____

Please submit a record of the settings of all your ion-optical elements (lenses, rod offsets, etc.) used to accomplish 10.

Note: Use the final Q2 stopping curve developed in instruction 10 to determine E_{50} (≡the Q2 rod offset that stops 50% of the projectile ions). For instructions 11–39 below, set the Q2 rod offset= (E_{50}−40) eV and set *all* the other ion-optical elements to the same values as were used for the final Q2 stopping curve of instruction 10.

Ion Intensity vs q_2:

Note: The q_2 values (referenced to q_3) must be varied in small increments to ensure that the measurements made here represent correctly the ion imaging occurring within your Q2Q3 structure (i.e., there may be severe oscillations in the ion intensity as q_2 is varied). These data will be used to make the necessary corrections for differences in the relative reaction pathlength and in relative transmission (cf. reference [14]).

Note: For instructions 11–17, verify that Q1 and Q3 are still set at their respective mass peak positions each time a different q_2 value is selected.

11. PIBON/TGOFF: Set Q1 and Q3 at the mass peak position for N_2^+. Measure the ion intensity at the mass peak position ($\simeq[N_2^+]_0$) as a function of q_2. Use values of q_2 between ca. 0.1 and 0.7. Record your measurements in the spaces provided.

$[N_2^+]_0$	_____	_____	_____	_____	_____	_____	_____	_____
q_2	_____	_____	_____	_____	_____	_____	_____	_____
$[N_2^+]_0$	_____	_____	_____	_____	_____	_____	_____	_____
q_2	_____	_____	_____	_____	_____	_____	_____	_____
$[N_2^+]_0$	_____	_____	_____	_____	_____	_____	_____	_____
q_2	_____	_____	_____	_____	_____	_____	_____	_____

12. PIBOFF/TGOFF: Measure the corresponding background intensity at just one value of q_2. _____
13. PIBON/TGON: Add sufficient SF_6 target gas so the ion intensity $[N_2^+]$ becomes ca. 0.7 $[N_2^+]_0$. Measure the ion intensity at the mass peak position for $N_2^+(\simeq[N_2^+])$ as a function of q_2. Use values of q_2 between ca. 0.1 and 0.7. Record your measurements in the spaces provided.

$[N_2^+]$	_____	_____	_____	_____	_____	_____	_____	_____
q_2	_____	_____	_____	_____	_____	_____	_____	_____
$[N_2^+]$	_____	_____	_____	_____	_____	_____	_____	_____
q_2	_____	_____	_____	_____	_____	_____	_____	_____
$[N_2^+]$	_____	_____	_____	_____	_____	_____	_____	_____
q_2	_____	_____	_____	_____	_____	_____	_____	_____

14. PIBOFF/TGON: Measure the corresponding background intensity at just one value of q_2. _____
15. PIBON/TGON: Set Q1 at the mass peak position for N_2^+ and Q3 at the mass peak position for SF_5^+. Measure the ion intensity at the mass peak position for SF_5^+ ($\simeq[SF_5^+]$) as a function of q_2. Use values of q_2 between ca. 0.1 and 0.7. Record your measurements in the spaces provided.

$[SF_5^+]$	_____	_____	_____	_____	_____	_____	_____	_____
q_2	_____	_____	_____	_____	_____	_____	_____	_____
$[SF_5^+]$	_____	_____	_____	_____	_____	_____	_____	_____
q_2	_____	_____	_____	_____	_____	_____	_____	_____
$[SF_5^+]$	_____	_____	_____	_____	_____	_____	_____	_____
q_2	_____	_____	_____	_____	_____	_____	_____	_____

16. PIBOFF/TGON: Measure the corresponding background intensity at just one value of q_2. _____
17. Submit the data and hardcopy plots for $[N_2^+]_0$ vs q_2, $[N_2^+]$ vs q_2, and $[SF_5^+]$ vs q_2.

ln *Y* and ln *W* Measurements:

Note: After you have found the tuning conditions that maximize SF_5^+ so that $[SF_5^+]\simeq[N_2^+]_0-[N_2^+]$, the same parameter settings (lens potentials, etc.) must be used for ln *W* measurements as are used for ln *Y* measurements. Only q_2 should be varied to tune to $q_{\text{react}}^{\max}$ for ion intensity measurements of N_2^+ and to $q_{\text{prod}}^{\max}$ for ion intensity measurements of SF_5^+.

All ln *Y*/ln *W* measurements within Part 2 should be done at the same time (cf. *Precaution* 6.). Record P/XQQ, and the other requisite measurements in the spaces provided. Please observe *Precaution* 8.

For $[N_2^+]/[N_2^+]_0 \simeq 0.6$:

18. PIBON/TGOFF: Set Q1 and Q3 at the mass peak position for N_2^+ with $q_2 = q_{react}^{max}$. Measure the ion intensity at the mass peak position ($\simeq[N_2^+]_0$). _____
19. Repeat 18, but with PIBOFF/TGOFF to measure the corresponding background intensity. _____
20. PIBON/TGON: Add sufficient SF_6 target gas so the ion intensity becomes $[N_2^+] \simeq 0.6\ [N_2^+]_0$. Measure the ion intensity at the mass peak position ($\simeq[N_2^+]$)._____ P/XQQ=_____.
21. Repeat 20, but with PIBOFF/TGON to measure the corresponding background intensity. _____
22. PIBON/TGON: Set Q1 at the mass peak position for N_2^+ and Q3 at the mass peak position for SF_5^+ with $q_2 = q_{prod}^{max}$. Measure the ion intensity at the mass peak position for SF_5^+ ($\simeq[SF_5^+]$). _____
23. Repeat 22, but with PIBOFF/TGON to measure the corresponding background intensity. _____
24. Repeat 18–23, but with sufficient SF_6 target gas so that $[N_2^+]/[N_2^+]_0 \simeq 0.8$. Record your measurements in the spaces provided for the corresponding instructions.

    "18."_____ "19."_____ "20."_____ "21."_____ "22."_____ "23."_____
    P/XQQ=_____

25. Repeat 18–23, but with sufficient SF_6 target gas so that $[N_2^+]/[N_2^+]_0 \simeq 0.7$. Record your measurements in the spaces provided for the corresponding instructions.

    "18."_____ "19."_____ "20."_____ "21."_____ "22."_____ "23."_____
    P/XQQ=_____

26. Repeat 18–23, but with sufficient SF_6 target gas so that $[N_2^+]/[N_2^+]_0 \simeq 0.9$. Record your measurements in the spaces provided for the corresponding instructions.

    "18."_____ "19."_____ "20."_____ "21."_____ "22."_____ "23."_____
    P/XQQ=_____

27. Repeat 18–23, but with sufficient SF_6 target gas so that $[N_2^+]/[N_2^+]_0 \simeq 0.6$. Record your measurements in the spaces provided for the corresponding instructions.

    "18."_____ "19."_____ "20."_____ "21."_____ "22."_____ "23."_____
    P/XQQ=_____

28. Repeat 20. _____ and 21. _____
29. Repeat 18. _____ and 19. _____

Detector's Conversion Gain Measurement:

You must make conversion gain measurements if your instrument uses analog current measurements. If your instrument uses *true* ion pulse counting (e.g., SCIEX TAGA 6000), conversion gain measurements are *not* needed [i.e., ignore this section (instructions 30–39)].

Warning: Some instruments use analog current measurements, but report the ion intensities as ion count rates within their data systems (i.e., the ion currents are converted to equivalent ion count rates via current-to-frequency converters or voltage-to-frequency converters or ?). Such instruments still require conversion gain measurements.

Here you will determine the ratio CG_{127}/CG_{28} for the conversion gain of SF_5^+ relative to that of N_2^+. However, to avoid complicating the conversion gain measurements, do not use SF_5^+. Instead, use n-butylbenzene (m/z 134) or other stable compound with a mass close to 127.

30. In general, follow the manufacturer's recommendations for conversion gain measurements. However, if your detector uses a conversion dynode, please observe the following additional precautions to ensure reproducible results.

Note: When making absolute current measurements with the detector turned on, use all the settings used for instructions 18–29. When you are using the Faraday cup (for absolute ion current measurements), turn off the detector's high voltage but use all the other settings used for instructions 18–29.

31. Make sure both the N_2 and the n-butylbenzene are flowing together into the ion source at all times. Use a fixed flow rate. Do 32–39 after the flows have stabilized (constant pressure in the ion source region).
32. PIBON/TGOFF: Set Q1 and Q3 at the mass peak position for N_2^+ with $q_2 = q_{react}^{max}$ for m/z 28. Leave everything turned on and monitor $[N_2^+]_0$ until it reaches the final (highest or lowest) stabilized ion current for $[N_2^+]_0$ (ca. 10–15 minutes).
33. PIBON/TGOFF: Set Q1 and Q3 at the mass peak position for 134^+ with $q_2 = q_{react}^{max}$ for m/z 134. Immediately record the initial absolute current measured for $[134^+]$ with the detector turned on.

    $I_{detector}$=_____ for m/z 134.

34. Repeat 32.
35. PIBON/TGOFF: Set Q1 and Q3 at the mass peak position for 134^+ with $q_2 = q_{react}^{max}$ for m/z 134. Immediately record the initial absolute current measured for $[134^+]$ with the Faraday cup.

    $I_{Faraday}$=_____ for m/z 134.

36. The ratio of $I_{detector}/I_{Faraday}$ from 33 and 35 provides an estimate for CG_{134}=_____.
37. Repeat 32–36, but use m/z 28 instead of m/z 134 in 33 and 35. For m/z 28, $I_{detector}$=_____ $I_{Faraday}$=_____ CG_{28}=_____
38. The values from 36 and 37 provide an estimate for the ratio CG_{134}/CG_{28}=_____.
39. Repeat 32–38 at least one more time to ensure your estimates for CG_{127}, CG_{28}, and CG_{127}/CG_{28} are reproducible.

Conclusion:

40. For each XQQ instrument, please submit:
    (1) this completed test protocol (i.e., with the blank spaces filled in)
    (2) a copy of the completed *Questionnaire*
    (3) any other data requested herein.
    Thank you.

Questionnaire

Note: Put a large asterisk (*) next to any proprietary (confidential) information which must not be divulged.

Participant's Name and Address: _____
_____
_____
_____
_____
Phone: _____

What type of XQQ instrument (QQ, QQQ, BEQQ, etc.)? _____
Manufacturer? _____ Model No.? _____
Does your XQQ instrument use a molecular beam target within Q2 (e.g., SCIEX TAGA 6000) or a collision cell enclosure surrounding Q2 (e.g., Finnigan TSQ70)?
Check one: Molecular beam _____ Collision enclosure _____
If a collision cell enclosure surrounds Q2, what is the rectilinear pathlength of the collision region (from the entrance aperture to the exit aperture)? _____cm

Quadrupole Rod Assemblies:

Is the Q1 quad rod assembly enclosed within a housing (enclosure) or uncovered (nude rods, no housing) within the vacuum chamber? Enclosed _____ Uncovered _____
Is the Q3 quad rod assembly enclosed within a housing (enclosure) or uncovered (nude rods, no housing) within the vacuum chamber? Enclosed _____ Uncovered _____
What is the rectilinear length of the Q2 quad rod assembly? _____cm
What is the field radius r_0 for the Q2 quad rod assembly? _____cm
If cylindrical rods are used for the Q2 quad rod assembly, what is the rod diameter? _____cm
Does each quad rod assembly (Q1, Q2, Q3) have its own separate rf/dc generator (quadrupole controller/power supply)? Yes _____ No _____
If you answered "No", which ones don't? Q1 _____ Q2 _____ Q3 _____
What is the frequency of operation for Q2? _____MHz
- (if variable frequencies are used for Q2, what nominal frequency was used for Ar^+? _____MHz for N_2^+? _____MHz for SF_5^+? _____MHz)

What is the frequency of operation for Q1? _____MHz
- (if variable frequencies are used for Q1, what nominal frequency was used for Ar^+? _____MHz for N_2^+? _____MHz for SF_5^+? _____MHz)

What is the frequency of operation for Q3? _____MHz
- (if variable frequencies are used for Q3, what nominal frequency was used for Ar^+? _____MHz for N_2^+? _____MHz for SF_5^+? _____MHz)

Interquadrupole Lenses:

Answer the questions below with reference to the following simplified schematic:

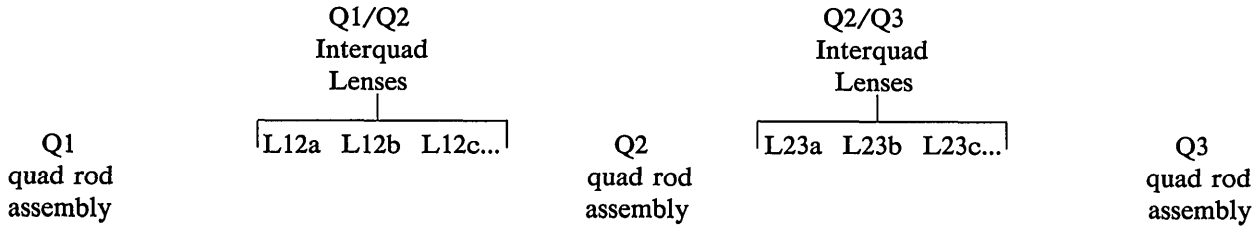

How many lenses are there betwen the Q1 quad rod assembly and the Q2 quad rod assembly (include the Q1 exit aperture and the Q2 entrance aperture in your count)? _____

What is the nominal diameter (in cm) of the aperture of each of the L12 interquadrupole lenses? L12a _____ L12b _____ L12c _____ L12d _____ L12e _____

If you are using a hybrid XQQ instrument (e.g., BEQQ, etc.), indicate the diameter (in cm) of the Q2 entrance aperture _____.

How many lenses are there between the Q2 quad rod assembly and the Q3 quad rod assembly (include the Q2 exit aperture and the Q3 entrance aperture in your count)? _____

What is the diameter (in cm) of the aperture of each of the L23 interquadrupole lenses? L23a _____ L23b _____ L23c _____ L23d _____ L23e _____

Modes of Operation:

Parent-scan mode: Q3 is set to a fixed mass while Q1 scans over a range of masses; one can thus assess which parent ion masses are the progenitors of a given daughter ion mass.

Daughter-scan mode: Q1 is set to a fixed mass while Q3 scans over a range of masses; one can thus assess which daughter ion masses are the progeny of a given parent ion mass.

For the parent-scan mode, how is the value of q_2 set in your instrument?

Check all that apply: It can be referenced to q_1? _____

It can be referenced to q_3? _____

Other? (Explain) _____

_____

For the daughter-scan mode, how is the value of q_2 set in your instrument?

Check all that apply: It can be referenced to q_1? _____

It can be referenced to q_3? _____

Other? (Explain) _____

_____

Comments:

About the Author: Richard I. Martinez is a research chemist in the Chemical Kinetics Division of the NIST Center for Chemical Technology.

References

[1] Busch, K. L., Glish, G. L., and McLuckey, S. A., Mass Spectrometry/Mass Spectrometry: Techniques and Applications of Tandem Mass Spectrometry, VCH, New York, 1988.
[2] Dawson, P. H., Quadrupole Mass Spectrometry and its Applications, Elsevier, Amsterdam, 1976.
[3] Dawson, P. H., Adv. Electronics Electron Phys. **53**, 153 (1980).
[4] Dawson, P. H., Int. J. Mass Spectrom. Ion Phys. **20**, 237 (1976).
[5] Dawson, P. H., and Fulford, J. E., Int. J. Mass Spectrom. Ion Phys. **42**, 195 (1982).
[6] Dawson, P. H., French, J. B, Buckley, J. A., Douglas, D. J., and Simmons, D., Org. Mass Spectrom. **17**, 205 (1982).
[7] Dawson, P. H., French, J. B., Buckley, J. A., Douglas, D. J., and Simmons, D., Org. Mass Spectrom. **17**, 212 (1982).
[8] Shushan, B., Douglas, D. J., Davidson, W. R., and Nacson, S., Int. J. Mass Spectrom. Ion Phys. **46**, 71 (1983).
[9] Martinez, R. I., Rapid Commun. Mass Spectrom. **2**, 8 (1988).
[10] Dawson, P. H., and Sun, W.-F., Int. J. Mass Spectrom. Ion Processes **55**, 155 (1983/1984).
[11] Martinez, R. I., and Dheandhanoo, S., Int. J. Mass Spectrom. Ion Processes **74**, 241 (1986).
[12] Martinez, R. I., and Dheandhanoo, S., J. Res. Natl. Bur. Stand. (U.S.) **92**, 229 (1987).
[13] Martinez, R.I., and Dheandhanoo, S., Int. J. Mass Spectrom. Ion Processes **84**, 1 (1988).
[14] Martinez, R. I., and Ganguli, B., Rapid Commun. Mass Spectrom. **2**, 41 (1988).
[15] Martinez, R. I., and Ganguli, B., unpublished work.
[16] Martinez, R. I., and Ganguli, B., unpublished work.
[17] Kaiser, E. W., Crowe, A., and Falconer, W. E., J. Chem. Phys. **61**, 2720 (1974).
[18] Paulson, J. F., Dale, F., and Studniarz, S. A., Int. J. Mass Spectrom. Ion Phys. **5**, 113 (1970).
[19] Amme, R. C., and Hayden, H. C., J. Chem. Phys. **42**, 2011 (1965).
[20] Futrell, J. H., Ed., Gaseous Ion Chemistry and Mass Spectrometry, Wiley, NY, 1986.
[21] Martinez, R. I., Rapid Commun. Mass Spectrom. **3**, 127 (1989).
[22] Dawson, P. H. and Sun, W.-F., Int. J. Mass Spectrom. Ion Phys. **44**, 51 (1982).
[23] Dawson, P. H. and Douglas, D. J., Int. J. Mass Spectrom. Ion Phys. **47**, 121 (1983).
[24] Dawson, P. H., Int. J. Mass Spectrom. Ion Phys. **50**, 287 (1983).

Volume 94, Number 5, September–October 1989
Journal of Research of the National Institute of Standards and Technology

A Cotinine in Freeze-Dried Urine Reference Material

Volume 94 Number 5 September–October 1989

Lane C. Sander and Gary D. Byrd

National Institute of Standards and Technology,
Gaithersburg, MD 20899

A cotinine in freeze-dried urine reference material (RM 8444) was prepared at three concentrations: (1) a "blank" level typical of nonsmokers with no exposure to cigarette smoke, (2) a "low" level corresponding to nonsmokers with passive exposure to side-stream smoke, and (3) a "high" level typical of smokers. Low- and high-level materials were prepared gravimetrically from pooled urine by the addition of appropriate amounts of cotinine perchlorate. Cotinine was determined by GC-MS using cotinine-d_3 as an internal standard. No evidence for sample inhomogeneity was observed. This reference material will fulfill a need for a urine-based standard to assist in the validation of field methods used for assessing exposure to cigarette smoke.

Key words: cotinine; cotinine perchlorate; GC-MS; passive smoking; side stream smoke; standards; tobacco.

Accepted: June 1, 1989

1. Introduction

The correlation of adverse health effects with cigarette smoking has been based largely on self-reported data of the number of cigarettes smoked [1]. The validity of such data, however, may be limited due to denial, which is common among young smokers and announced quitters [2–4]. In addition, variables such as the "strength" of the cigarette (tar and nicotine levels), depth and frequency of inhalation, and duration of smoking affect the dose received by the smoker [2,5,6]. In studies involving passive exposure of nonsmokers to side-stream cigarette smoke, self-reported data are not applicable. Related problems exist in quantification of intake of smokeless tobacco products. Other studies have examined the exposure of infants to nicotine via milk from smoking mothers [7,8]. It is clear that an objective measure of exposure to cigarette smoke is needed to permit correlation of physiological changes with smoking.

A variety of compounds have been proposed as epidemiological markers for cigarette smoke exposure [2,9]. Cigarette smoke consists of a complex mixture of particles and gases containing appreciable quantities of nicotine, carbon monoxide, and hydrogen cyanide. These compounds and their metabolites are present in biological fluids (serum, saliva, urine) of smokers. Carbon monoxide is present as carboxyhemoglobin (COhb), and has a biological half-life of 2–4 h [10]. Because of this small half-life, COhb levels reflect only recent exposure to cigarette smoke. Environmental contributions of carbon monoxide further complicate interpretation and use of this marker. The half-life of nicotine is even shorter (30–80 min) [11] and thus reflects only transient exposure. Cumulative exposure is better correlated with serum thiocyanate levels (half-life 14 d) [12] resulting from transformation of hydrogen cyanide. Unfortu-

nately, thiocyanate levels are also affected by diet, limiting its usefulness as an epidemiological marker. Perhaps the best single measure of cumulative exposure to tobacco products is given by cotinine [13]. Cotinine ((S)-1-methyl-5-(3-pyridinyl)-2-pyrrolidinone) is the major metabolite of nicotine. It has a biological half-life of approximately 20 h [14] and is found in the serum and urine of smokers. Cotinine levels are linearly and directly related to nicotine intake [5].

To assist in the validation of the accuracy of analytical methods for the determination of cotinine in urine, a freeze-dried urine containing cotinine was prepared for use as a reference material. This reference material, designated RM 8444, consists of three lots of freeze-dried urine containing different concentrations of cotinine: (1) an unspiked "blank" level, (2) a "low" level (approximately 50 ppb), and (3) a "high" level (approximately 500 ppb). These cotinine concentrations represent the levels that might be expected in nonsmokers with no exposure to cigarette smoke (or related nicotine containing products), nonsmokers with passive exposure to side-stream smoke, and smokers, respectively. The low- and high-level materials were prepared gravimetrically by spiking urine with known quantities of cotinine perchlorate; the blank level material was unspiked. Because these reference materials are homogenous and well characterized, they are useful for verifying methods for the determination of cotinine in urine.

2. Experimental Section

2.1 Cotinine Standards

Because the free-base form of cotinine is hygroscopic, cotinine perchlorate was used as the primary standard for this work. Cotinine perchlorate was unavailable commercially and was synthesized from cotinine (Aldrich Chemical Co.[1], lot 04112MT) and 70% perchloric acid, using the method of Jacob and Benowitz [15]. One g cotinine was distilled under vacuum at 225 °C. The product was dissolved in 15 mL isopropanol and added to 1 mL perchloric acid in 15 mL isopropanol. A white precipitate formed which dissolved upon swirling and reformed when cooled in an ice bath. The crystals were filtered and washed with portions of isopropanol and ethyl ether. After air drying, the product was dried under reduced pressure for 1 h.

Purity was determined by differential scanning calorimetry over the temperature interval 210–220 °C. The purity was determined to be 99.91 mol percent (melting point 218 °C). Also, the melting point was measured in a glass capillary, and crystals were observed to melt over the range 212–216 °C (cotinine perchlorate mp=218 °C [15]). No evidence of organic impurities was observed by liquid chromatography (LC) or gas chromatography (GC) analyses. A sample of the product was submitted to Galbraith Laboratories (Knoxville, TN) for elemental analyses. Duplicate determinations were made for carbon, hydrogen, nitrogen, chlorine, and oxygen (see table 1). Based on the molecular formula for cotinine perchlorate, expected elemental percentages can be calculated. As shown in table 1, the measured composition compares favorably to the calculated values. On the basis of these characterizations, product purity was accepted to be greater than 99%, and no corrections for sample impurity were made.

Deuterated cotinine (cotinine-d_3) was obtained from Cambridge Isotope Laboratories (Woburn, MA). The isotope purity determined by gas chromatography- mass spectrometry (GC-MS) was 98.7%. Corrections were made for the amount of undeuterated cotinine contributed, in all calculations. Because deuterated cotinine was obtained in the free-base form and readily absorbs water, the resultant weight gain makes it impossible to know the actual concentration of the internal standard spiking solution. The approximate concentration of this solution (12.4 ppm) was only used to make minor corrections to the response factors involving isotopic purity of the internal standard. The same internal standard solution was used throughout this study for both unknowns and response factor solutions. Response factors were determined using four independently prepared calibration solutions.

2.2 Preparation of Reference Materials

Cotinine reference materials were freeze dried. Samples from two freeze-drying runs were used for each of the low- and high-level spiked materials, and three runs for the blank material. Separate urine collections were made for the three materials. Donors (nonsmokers) were advised to avoid any exposure to tobacco smoke or caffeine for at least 48 h prior to the collection. Although caffeine does not interfere in GC-MS determinations of cotinine,

[1] Certain commercial equipment, instruments, or materials are identified in this report to specify adequately the experimental procedure. Such identification does not imply recommendation or endorsement by the National Institute of Standards and Technology, nor does it imply that the materials or equipment identified are necessarily the best available for the purpose.

Table 1. Elemental composition of cotinine perchlorate[a]

Element	Calculated composition	Analysis #1	Analysis #2	Calculated purity (%)
carbon	43.41	43.56	43.28	100.3, 99.7
hydrogen	4.74	4.97	4.92	104.9, 103.8
nitrogen	10.13	10.20	10.06	101.7, 99.3
chlorine	12.81	12.60	12.88	98.4, 100.5
oxygen	28.91	28.64	28.71	99.1, 99.3

[a] Elemental composition determinations performed by Galbraith Laboratories, Knoxville, TN.

the level of caffeine was reduced so as not to preclude the use of any liquid chromatographic methods (liquid chromatography was not used in the analysis of this reference material). Multiple urine pools were used (as opposed to a single urine pool) to avoid problems in storing the urine between the freeze-drying runs. Five mL aliquots of each of the urine samples were pipetted into 10-mL capacity serum cap vials. Excess material (a total in each case of about 8–9 L) was prepared to facilitate handling and to promote sample homogeneity.

Cotinine in urine materials were prepared gravimetrically using cotinine perchlorate for the low- and high-level solutions. Cotinine was not added to the blank-level material. For low- and high-level materials, an appropriate amount of cotinine perchlorate was weighed and dissolved in approximately 5-mL distilled water. This solution was transferred quantitatively to the pooled urine through a thistle tube using successive washings with water (total volume of solution added was approximately 125 mL). The final weight of spiked urine was recorded and the solution was stirred for at least 2 h before pipetting. Gravimetric values for the solutions are listed in table 2.

2.3 Freeze-Drying Procedure

Five-mL aliquots of the urine materials were pipetted into 10-mL serum cap vials using an automatic pipetter. About 1200 units were prepared at each concentration level. Prior to freeze-drying, the samples were frozen at −80 °C. The freeze-drier was cooled to −50 °C (shelf temperature) in preparation to receive the samples (condenser at −70 °C). The two trays were rapidly transferred from the freezer to the freeze drier to minimize any warming of the samples. Two temperature probes were used per tray, with probe placement at the center and edge of each tray. Immediately after transfer, the freeze drier was evacuated to start the freeze-drying process. Pressures were typically about 13 Pa (100 μm Hg). During the initial pump down, sample foaming was observed in a fraction of the samples; foaming was most prevalent in samples near the edges of the trays (in "warm" samples).

The shelf temperature was set and maintained at −30 °C for the first 24 h period. This temperature was increased in roughly 15° increments every 12 h period. The temperature, as monitored by the probes, changed only slightly during the first 36 h.

Table 2. Gravimetric and GC-MS values for spiked cotinine in urine reference materials

Level	Weight solution	Weight cotinine perchlorate	Conc. cotinine[a] gravimetric	Conc. cotinine[a] (original)	Conc. cotinine[a] (160 d)
blank	8648 g			0.8±0.3 ng/g	
low	6808 g	0.593 mg	55.47 ng/g	56 ± 2 ng/g	52± 3 ng/g
high	7361 g	5.662 mg	489.88 ng/g	491 ± 6 ng/g	485±12 ng/g

[a] Cotinine concentration values are corrected for the weight of the perchlorate salt.

Freeze drying was considered complete when the shelf and probe temperatures were at ambient temperature, and the pressure was less than 13 Pa. The freeze-dried samples were sealed with the serum cap tops under a slight negative pressure. Total time to freeze dry each batch was about 72 h. Two freeze-drying runs were required for each reference material level.

2.4 Analysis by GC-MS

A solution of cotinine-d_3 (approximately 12.4 ppm) was prepared in methanol and was ampouled for later use. This solution was used as an internal standard for both calibration standards (response factor solutions) and for the unknowns (urine reference materials). Four separate response factor solutions were prepared. Independent response factors were determined for each level. Separate response factors were calculated for m/z 98/101 and 176/179, and cotinine concentration values were determined based on both mass pairs.

Six vials from the low- and high-level materials were selected by a stratified random sampling scheme. Due to the very low cotinine level in the blank material, special procedures were required to estimate the cotinine in these samples (described below). The spiked urine materials were reconstituted by adding 5 mL of distilled water to each vial, followed by shaking and sonication for 60 s. Each sample was spiked with 50 μL of cotinine-d_3 internal standard solution, followed by an addition of 10 drops of 10 *M* KOH. The samples were then extracted with 5 mL of methylene chloride. The methylene chloride layer was removed with a pipet and treated with 1–2 g of sodium sulfate. The methylene chloride was decanted into a centrifuge tube and evaporated to dryness under argon. The residue was dissolved in 50 μL of methanol and analyzed by GC-MS.

A DB-210 250 μm i.d. capillary column (J & W Scientific, Folsom, CA) was used for the GC-MS analysis of the urine extracts. This column is more polar than the more conventional DB-5 phase, and yields a better peak shape than the DB-5 phase. The following temperature program was used in the GC separation: 185 °C initial, linear ramp of 5 °C/min, final temperature of 225 °C. Between GC runs, the column was briefly ramped to 230 °C. Four masses were monitored: 176, 179, 98, and 101, corresponding to parent ions and major fragments from cotinine and cotinine-d_3. A typical separation of a urine extract is illustrated in figure 1.

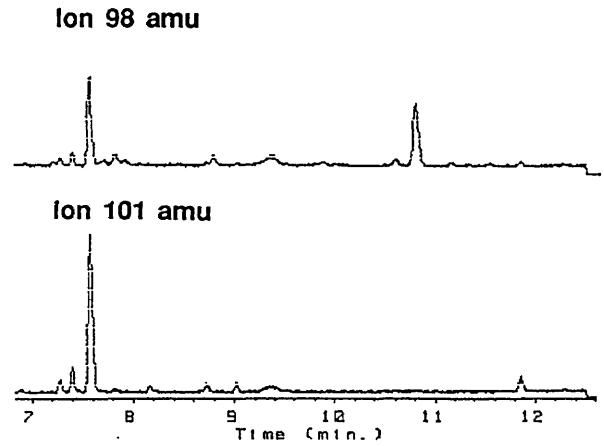

Figure 1. GC-MS determination of cotinine in reference material 8444. Ion chromatograms for mass fragments 98 (cotinine) and 101 (cotinine-d_3) are shown.

To obtain an estimate of the concentration of cotinine in the unspiked urine blank, 50 mL (10 vials) of urine were combined. Ten vials from the beginning, middle, and end of the blank preparation were analyzed. The uncertainty of this determination is high due to the small areas measured (signals were only a few times the noise level). The average result of the determinations is given in table 2.

2.5 Stability

Cotinine levels were again determined after a storage period of 160 d. During this time the materials were stored at ambient temperature for ~4 months, and at −20 °C for ~1 month. Cotinine levels were determined for low and high level samples as described above. The results of the determination are listed in table 2. Cotinine levels were found to be slightly lower than previously determined, however the values were still within the uncertainty of the measurement.

3. Results

3.1 Discussion

Careful examination of table 2 reveals that no significant difference exists between the values determined by gravimetry and GC-MS, for low- and high-level samples. Essentially all of the spiked cotinine (within measurement error) is recovered upon reconstitution of the sample. The cotinine concentrations calculated from gravimetric measurements are thus confirmed by independently de-

termined values from GC-MS measurements. Cotinine concentrations determined after 160 d were similar to those determined originally, however small decreases in concentration were observed (see table 2). Possible sources for these decreases could include analyte degradation or irreversible adsorption onto particulate or other matter. Because the samples were stored at ambient temperature for approximately 4 months, it is possible that changes in cotinine concentration occurred at that time. Stability of this reference material should be enhanced by storage at or below 0 °C. Cotinine levels will be assessed periodically to assure that the concentrations remain within recommended ranges.

3.2 Recommended Values

The following recommended cotinine concentrations for the three reference materials are based only on the GC-MS determinations.

blank level: 0.8 ± 0.3 ng/g

low level: 52^{+2}_{-5} ng/g

high level: 485^{+4}_{-10} ng/g

These values are based on judgment, and reflect measurement uncertainties and possible sample instability. Average cotinine concentrations compare very favorably to the gravimetric values, and are within the error of the determination. It is clear that losses of the analyte due to freeze drying were negligible. No evidence of sample inhomogeneity was observed for any of the materials.

About the authors: Lane Sander is a research chemist in the Center for Analytical Chemistry, National Institute of Standards and Technology. Gary Byrd is currently a senior research chemist at R. J. Reynolds Tobacco Company.

4. Acknowledgments

This work was funded under contract (DW13933291-01-0) by the Environmental Protection Agency, Environmental Monitoring Support Laboratory, Las Vegas. The authors thank Richard Christensen for performing the differential scanning calorimetry measurements.

5. References

[1] Haley, N. J., Axelrad, C. M., and Tilton, K. A., Am. J. Public Health **73**, 1204 (1983).
[2] Hill, P., Haley, N. J., and Wynder, E. L., J. Chron. Dis. **36**, 439 (1983).
[3] Allen, P., Lundl, B., and Westling, H., Psychopharmacology **49**, 263 (1976).
[4] Gillies, P. A., Wilcox, B., Coates, C., Kristmundsdotir, F., and Reid, D. J., J. Epid. and Commun. Health **36**, 205 (1982).
[5] Galeazzi, R. L., Daenens, P., and Gugger, M., J. Clin. Pharmacol. **28**, 301 (1985).
[6] Hill, P., and Marquardt, H., Clin. Pharmacol. Ther. **27**, 652 (1980).
[7] Luck, W., and Nau, H., J. Pediatrics **107**, 816 (1985).
[8] Luck, W., and Nau, H., Br. J. Clin. Pharmacol. **18**, 9 (1984).
[9] Vesey, C. J., Saboojee, Y., Cole, P. V., and Russell, M. A. H., Brit. Med. J. **284**, 1516 (1982).
[10] Wald, N., Howard, S., Smith, M. G., and Bailey, A., Thorax **30**, 133 (1975).
[11] Issac, P. G., and Rand, M. J., Nature **236**, 308 (1972).
[12] Prue, D. M., Martin, J. E., and Hume, A. S., Behav. Ther. **11**, 368 (1980).
[13] Benowitz, N. L., Hall, S. M., Herning, R. I., Jacob, P., Jones, R. T., and Osman, A. L., N. Engl. J. Med. **309**, 139 (1983).
[14] Feyerabend, C., Bryant, A. E., Jarvis, M. J., and Russell, M. A. H., J. Pharm. Pharmacol. **38**, 917 (1986).
[15] Jacob, P., and Benowitz, N. L., Cotinine Analytical Workshop (EPA), Research Triangle Park, NC, November 10–11, 1986.

Volume 94, Number 5, September–October 1989
Journal of Research of the National Institute of Standards and Technology

The NIST Automated Computer Time Service

Volume 94 Number 5 September–October 1989

J. Levine, M. Weiss, D. D. Davis, D. W. Allan, and D. B. Sullivan

National Institute of Standards and Technology,
Boulder, CO 80303

The NIST Automated Computer Time Service (ACTS) is a telephone time service designed to provide computers with telephone access to time generated by the National Institute of Standards and Technology at accuracies approaching 1 ms. Features of the service include automated estimation by the transmitter of the telephone-line delay, advanced alert for changes to and from daylight saving time, and advanced notice of insertion of leap seconds. The ASCII-character time code operates with most standard modems and computer systems. The system can be used to set computer clocks and simple hardware can also be developed to set non-computer clock systems.

Key words: automation; computers; delay; digital systems; frequency; propagation delay; telephone; synchronization, time.

Accepted: July 24, 1989

1. Introduction

The principal limitation to the accuracy of most methods of time dissemination is the uncertainty in the velocity of propagation of the information through the medium separating the transmitter and receiver. The delay, which is typically on the order of milliseconds, depends both on the physical length of the path and on the group velocity of the signal, and neither of these is well known in general. Either the path length or the group velocity is likely to change with time, so that real-time measurements of the transit time are generally required if the highest accuracy is to be realized. The telephone system provides a unique environment in this respect, since such measurements can be made using simple hardware. Using the telephone system for time dissemination is also desirable since telephone service is already provided to most homes, businesses, and laboratories.

If a passive timing receiver is replaced by an active transponder, the time delay along the path can be determined from the transmission end by sending a pulse to the user and measuring the delay until the echoed pulse returns. Half of this round-trip delay is the time for the signal to reach the user assuming that the communication medium is reciprocal (i.e., that the delay is the same in both directions). This is not always the case for atmospheric paths because of fluctuating multi-path effects and asymmetries in the antennas, and it was not always the case in the past for telephone circuits. It was not uncommon to see telephone connections involving, for example, one-way connection by land-line and the other by satellite. In recent years the telephone carriers have moved away from this practice and now prefer to route both directions of transmission along the same path. As will be seen later in this paper, tests indicate that the telephone path is highly reciprocal.

With this as background and with growing interest in millisecond-level synchronization of comput-

ers, NIST has developed a simple telephone system for automated setting of clocks in digital systems. The system makes no demands on the receiver and will function with both passive receivers and active transponders. A passive receiver consists of a modem and a terminal, computer or other display device. An active transponder consists of the same hardware with the additional capability of being able to echo the received messages back to NIST using either hardware or software methods. For either type of system, the modem must conform to either the Bell 103A standard for frequency-shift keying at 300 bits/s or the Bell v212a standard for phase-shift keying at 1200 bits/s. The terminal, computer or display device must recognize the standard ASCII code transmitted with 7 data bits, space parity and 1 stop bit.

The current telephone number for the service is (303) 494-4774. This is not a toll-free number. The following sections describe the service in more detail including discussion of (1) the operation of the service, (2) the reliability of the transmission system and, (3) software and hardware which have been developed for the user end.

2. Operation of ACTS

2.1 Transmission formats

The transmission format at 1200 bits/s is shown in figure 1.

a. The column labeled MJD is the Modified Julian Day number, which advances by 1 at 0000 Coordinated Universal Time (UTC) every day. The MJD corresponding to 1 January 1989 was 47527.

b. The next six numbers give the Coordinated Universal time as: years since 1900, month, day, hour, minute and second. Coordinated Universal Time is the official international time and was formerly called Greenwich mean time.

c. The column labeled DST is a flag used to specify if a correction for daylight saving time is required now or is imminent. This flag is valid for most of the continental United States. If DST is 00 then standard time is in effect. If DST is 50 then daylight saving time is in effect. If DST is between 99 and 51 then a transition *to* daylight saving time is approaching. Daylight saving time will be in effect at 2:00 (2:00 a.m.) local time on the day when the count reaches 51. If DST is between 49 and 01 a transition *from* daylight saving time back to standard time is approaching. It will arrive at 2:00 (2:00 a.m.) local time on the day when the counter is 01. In either transition situation, the counter is decremented at 00:00:00 (midnight) UTC every day.

d. LS is the leap-second flag and is normally 0. It will be set to 1 to indicate that a leap second is to be added following 23:59:59 UTC on the last day of the current month. This second will be named 23:59:60 UTC, and the second following it will be 00:00:00 of the following day. The LS flag will be set to 2 to indicate that a second is to be dropped at

?=Help
National Institute of Standards and Technology
Telephone Time Service

(1 second pause here)

MJD	YR MO DA	H M S	DST	LS	DUT1	msADV		OTM
47222	88 - 03 - 02	21:39:15	83	0	+.3	045.0	UTC(NIST)	*
47222	88 - 03 - 02	21:39:16	83	0	+.3	045.0	UTC(NIST)	*
47222	88 - 03 - 02	21:39:17	83	0	+.3	045.0	UTC(NIST)	*
47222	88 - 03 - 02	21:39:18	83	0	+.3	045.0	UTC(NIST)	*
47222	88 - 03 - 02	21:39:19	83	0	+.3	037.6	UTC(NIST)	#
47222	88 - 03 - 02	21:39:20	83	0	+.3	037.6	UTC(NIST)	#

etc...etc...etc.....

Figure 1. Time code and time marker transmitted by ACTS at 1200 bits/s. The abbreviations are as follows: MJD=Mean Julian Date, YR=Year, MO=Month, DA=Day, H=Hour, M=Minute, S=Second, DST=Daylight Saving Time (a flag meaning that a change is coming), LS=Leap Second (a flag meaning a leap second is to be added), DUT1=UT1−UTC (earth rotation time minus coordinated universal time), msADV=milliseconds of advance of the time marker, OTM=On-Time Marker.

end of the last day of the current month. The second following 23:59:58 UTC will be 00:00:00 UTC of the next day. Added leap seconds are generally required about every 18 months to maintain the coordination of UTC; it is unlikely that seconds will be dropped in the forseeable future.

e. DUT1 is the approximate difference between a time scale defined in terms of the rotation rate of the earth (UT1) and UTC. That is, DUT1 = UT1 − UTC. The difference is given to the nearest 0.1 s.

f. msADV is the advance of the on-time marker in milliseconds. The center of the stop-bit of the on-time marker leaves the transmitter early by this amount so as to arrive at the user on-time. The method used to estimate this parameter and the uncertainty of this estimate are discussed below.

g. OTM is the on-time marker. It is either "*" or "#" as discussed below. The center of the stop-bit of this character is intended to arrive at the user at the time specified by the previous characters on the same line.

A help message is available if the user sends a question mark early in the transmission. This, however, preempts the transmission of time information for the rest of that call.

The transmission format at 300 bits/s is similar, but there is not enough time to send the entire message. The transmission consists of the UTC time in hours, minutes and seconds, the current advance in milliseconds and the on-time marker. In the future, alternating halves of the full message may be sent every second together with an on-time marker, so that the full date can be decoded every 2 s.

2.2 Modes of Operation of the Service

Depending on the user equipment, the ACTS service provides three modes for checking and/or setting computer clocks.

- In the simplest form of the service, a passive user receives the time code and the on-time marker/character but does not echo the received message. In this case, an advance of 45 ms is used for all transmissions. The OTM should arrive at the user within 100 ms of the correct time unless the connection is routed through a satellite.
- If the user echoes all characters back to NIST, the round-trip line delay of the on-time marker will be used to adjust the advance of subsequent transmissions. The accuracy in this mode should be better than 10 ms and the repeatability is about 1 ms.
- If 300 bit/s modems are used and the user echoes all characters back to NIST, the slower transmission speed means that the full time code is not transmitted, but the measured delay is likely to be more accurate. Our experience indicates that the accuracy will be approximately 1 ms.

In any of these modes, the maximum connection time is 55 s. If all of the lines are busy at any time, the oldest call will be terminated if it has been on line more than 15 s, otherwise the call that first reaches 15 s is disconnected.

2.3 Reliability

To help ensure that ACTS never sends the wrong time, the system has triple redundancy and special self checking to enhance reliability and to increase the volume of calls that can be handled. The basic unit (see fig. 2) consists of three time-code generators, each with a complete system for generating the time-code and disseminating it through a separate modem to one of the telephone lines. Each of the time-code generators receives an independent time signal from a different clock in the NIST time scale. The time code needs to be initialized by an operator, but is automatically updated by the hardware after that. The power supply for the system is backed up by batteries so that the internal clocks do not lose time during a power failure.

Each time-code generator constantly compares its own time code with the codes of the other two, and participates in majority voting on the correctness of these codes. The time code is transmitted at 100 bits/s from each generator to the other two. This code contains all of the information transmitted through the telephone line. Each generator compares the bits of the two incoming codes with its own code and flags a generator as bad if any one disagrees with the other two. The flag of one generator declaring another bad is passed to a central control module as a vote against the offending generator. If any two of the generators vote against any single generator, the loser is taken off line. If all three disagree with one another, all three are disabled.

Each time-code generator receives a timing signal from the other two and compares these signals with its own internal time. If either time difference is larger than 15 μs, this is reported to the control module. Again, the votes are counted by the control module. A vote of two to one takes the loser off line and disagreement among all three disables all of them.

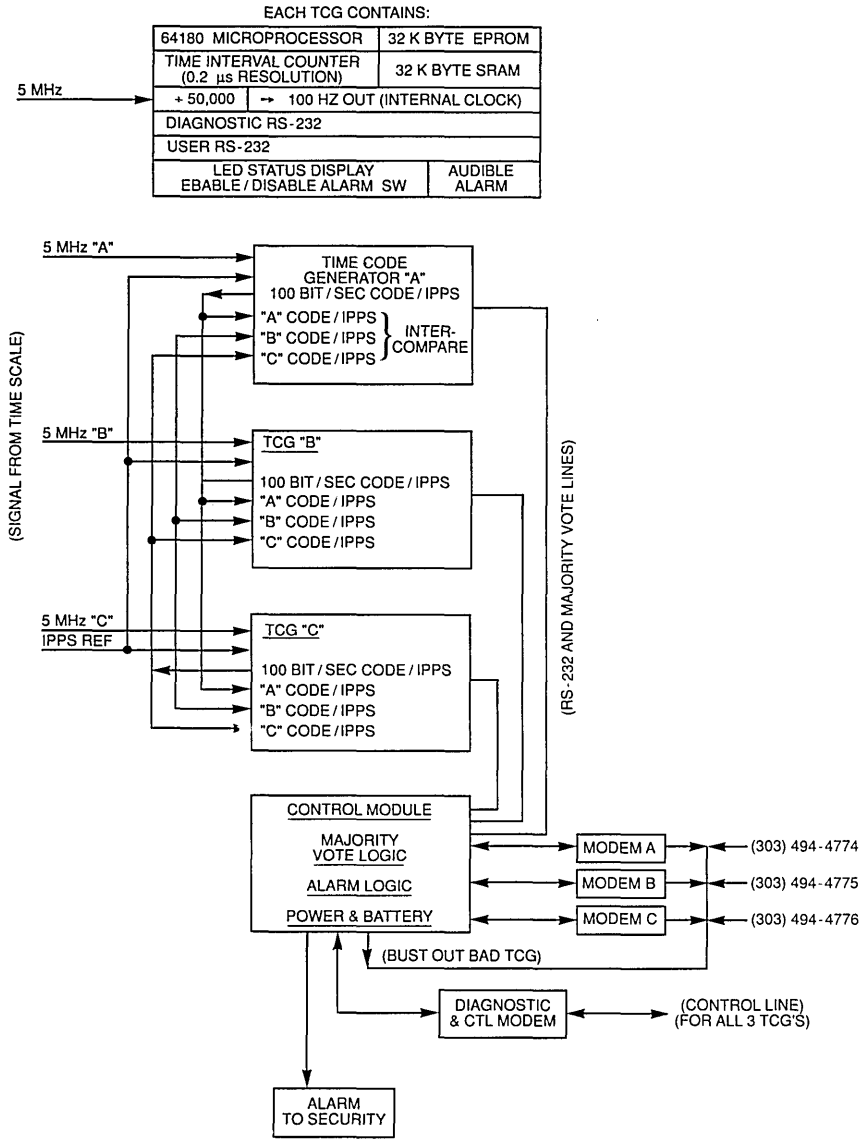

Figure 2. Block diagram of the ACTS transmitter including time-code generators and control module.

If an individual time-code generator finds either a code or a time error it sounds an audible alarm. If there is total disagreement among the three generators, all three generators are taken off line and the lines to these generators are set so that a caller will receive a busy signal. The system is also connected to a special alarm at the Boulder NIST security office and signals that office if problems develop. This office then contacts one of the system operators, either at work or at home. To facilitate operations and service, the system can be operated remotely using extensive control and diagnostic functions.

The ACTS system can be expanded in three-line units, each operating independently in the manner described above. If an entire three-generator unit is taken off-line, then the effect is to reduce the number of available lines by three. The desired effect is that the system transmits nothing rather than transmitting a code or time marker which is in error.

3. User Software and Hardware

3.1 Software

We have developed some example ACTS software which runs on a number of popular computers—for IBM PC/XT/AT and compatible systems[1], for the DEC PDP-11, and for Sun systems. There has been no attempt to be comprehensive in coverage of different computers, but rather to focus on a few example packages which can then be adapted to other machines. The NIST software provides for automated dialing, selection of time zone, selection of mode of operation, echoing of the OTM, setting of the computer clock, archiving of clock offset, and transmission to the port of the computer of a signal which can be used to produce an external time pulse coincident with the OTM. The program is written in a modular fashion so that additional features, such as a graphical presentation of the time-difference data or a more comprehensive statistical analysis of the performance of the local clock, can be added easily. This example software (which includes source code) is available on a $5\frac{1}{4}$-in, 360-kbyte MSDOS diskette along with instructions for $35.00. To order this software contact:

NIST Office of Standard Reference Materials
B311 Chemistry Building
Gaithersburg, MD 20899
(301) 975-6776

Specify that you want RM 8101, software for Automated Computer Time Service.

3.2 Hardware

Using software developed by NIST, the PC/XT/AT compatibles will deliver a signal coincident with the OTM to the parallel printer port. The very simple circuit shown in figure 3 can be used to convert this to a positive pulse. This might be useful for synchronizing an external system or for starting or stopping a counter in a precise measurement of frequency (see sec. 5). A second circuit which we have tested (see fig. 4) echoes all characters from the user and provides an external pulse when the OTM is received. This circuit, which allows ACTS to calibrate the phone line and advance the OTM accordingly, requires an external modem, but does not require a computer. To use this circuit, the user must first manually establish the telephone connection with NIST.

[1] Certain commercial equipment, instruments, and materials are identified in this paper in order to adequately specify the experimental procedure. In no case does such identification imply recommendation or endorsement by the National Institute of Standards and Technology, nor does it imply that the material, instruments, or equipment identified is necessarily the best available for the purpose.

4. Timing Accuracy

Since there are many different ways of using the ACTS system, it is not possible to estimate the timing accuracy in general. The following discussion estimates the major contributions to the error budget for many common configurations. Only the most important sources of error are discussed; uncertainties (such as cesium clock performance or variability in the cable delays) whose contribution to the error budget would be less than 1% of the total have been ignored.

4.1 Transmitting and Receiving Hardware

The on-time marker is a standard ASCII character which is sent to the user in a standard bit-serial format. Before the start of the transmission, the output line is held at a voltage corresponding to a binary 1. The transmission begins with a binary 0 start bit, the 8 bits that specify the character and a binary 1 stop bit. The 8 character bits are sent with the least significant bit first; the most significant bit, which is sometimes used as a parity bit, is always 0. The binary representations of the transmissions for the two types of on-time marker are 0 01010100 1 for * and 0 11000100 1 for #. In both cases, the center of the final 1 bit is intended to arrive on time. Each bit is 3.3 ms long at 300 bits/s and 833 μs at 1200 bits/s. The timing of the bits is set by a crystal-controlled oscillator operating at 64 times the bit rate, and the center of the on-time marker can be uncertain by ±0.5 cycle of this oscillator. The corresponding timing uncertainties are thus about 52 μs at a transmission speed of 300 bits/s and 13 μs at 1200 bits/s.

The receiving hardware operates in a similar manner, beginning asynchronously when the leading edge of the start bit is sensed and assembling the bits of the character using a local oscillator which usually operates at 16 times the bit rate. The process ends when the center of the stop bit has been reached. The center of the stop-bit of the on-time marker can be uncertain by ±0.5 cycle of the

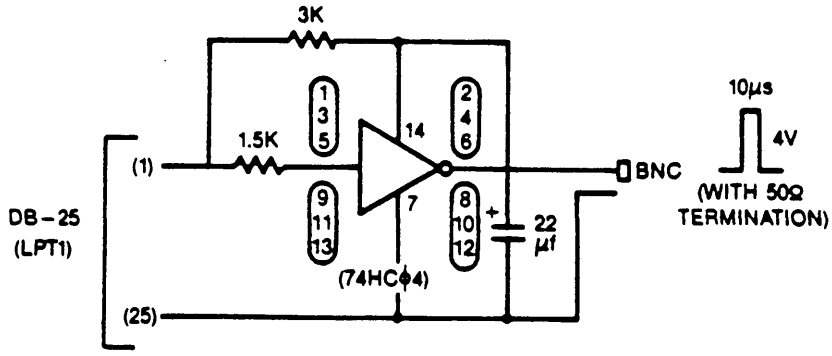

Figure 3. Simple circuit used to obtain a positive pulse coincident with the OTM from any PC/XT/AT compatible computer using the NIST software. The HCMOS invertor can be built directly into a DB-25 male connector.

receiver oscillator, which corresponds to an uncertainty of 208 μs at a transmission speed of 300 bits/s and 52 μs at 1200 bits/s. The transmitter and receiver clocks are not related; the mean value of the combined uncertainty is about 215 μs at 300 bits/s and 54 μs at 1200 bits/s.

4.2 Modems

4.2.1 Transmission at 300 bits/s To transmit and receive data at 300 bits/s, the modems use frequency-shift keying. The originating modem sends 1270 Hz for a binary 1 and 1070 Hz for a binary 0. The receiving modem sends 2225 Hz for a binary 1 and 2025 Hz for a binary 0. Since the line operates in full-duplex with both channels active simultaneously, the frequency slew-rate of the modulator must be controlled to prevent interference between the two channels. In both cases, the receiver must distinguish between two frequencies that are 200 Hz apart in a time that must be shorter than (or at most equal to) the bit-duration time of 3.3 ms. Our measurements indicate that typical discrimination times are about 1 ms; these measurements may vary by as much as 20% depending on signal strength and other factors.

The modem standards do not specify the methods to be used for either the modulator or the demodulator, and some variation in group delay is to be expected among different designs. If the modem does not contain a scrambler, the modem delays are on the order of the bit period and the asymmetry in the two directions is unlikely to exceed 1 ms.

4.2.2 Transmission at 1200 bits/s These higher speed modems use phase-shift keying to transmit the information. Pairs of bits are combined to form *dibits*; each dibit specifies one of four possible phase shifts that is to be applied to the carrier. The 1200 bit/s data rate is transmitted using one-half that number of phase-transitions/s so that the telephone line and phase detector must operate at 600 Baud. Since the phase of the carrier is significant, the bit-clocks in the transmitting and receiving modems must have the same frequency *and phase*. The asynchronous data bits must be synchronized with this clock, unlike the frequency-shift system described above where the synchronization is with respect to a clock with a frequency much higher than the bit rate.

The bandwidth required by these modems is generally broad enough to require some form of equalization to compensate for variations in the group delay of the telephone circuit with frequency. The equalizer coefficients are adjusted for random input data by transmitting a densely spaced line spectrum when the connection is first established and during idle periods thereafter. These calibration signals are generated by means of digital scramblers—shift-register circuits with feedback whose output is a function of both the current input and the previous transmissions.

The designs of the scramblers, the equalizers and the synchronizers have been widely discussed in the literature, and our interest in them is limited to their effects on the group delay of the transmission, and especially on its asymmetry. The basic delay through a scrambler/de-scrambler combination is about 30 ms and the average value of the offset produced by the synchronization of the asynchronous input data to the transmitter clock is 0.5 clock periods or 417 μs. Although the design of the scrambler is defined by the modem standards, the

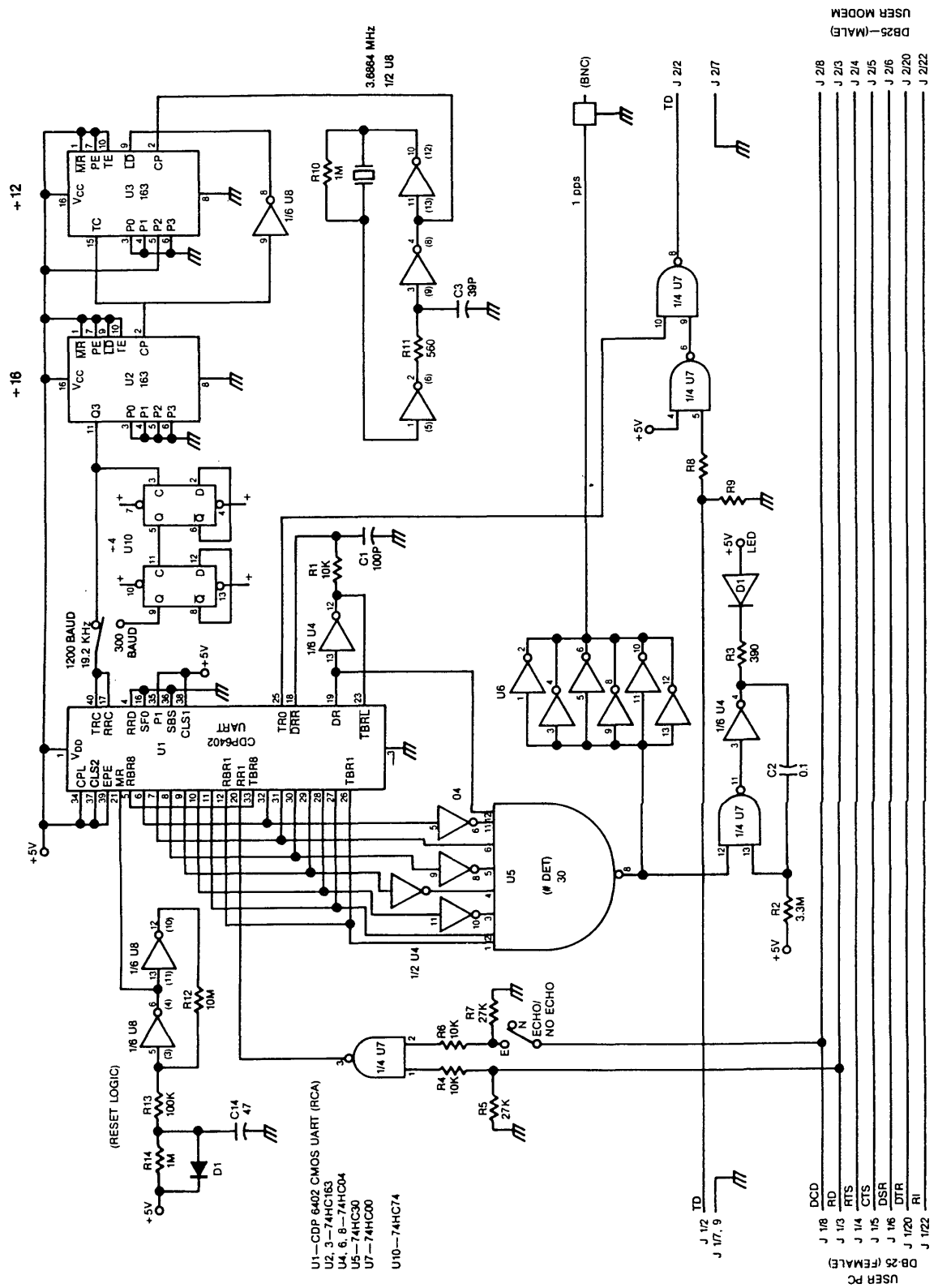

Figure 4. This circuit can be connected directly to a modem or can be bridged across the PC-to-modem cable. An output pulse is generated when the "#" OTM is received. This does not require any special software for the PC.

design of the equalizer is not, and combinations of modems from different suppliers may exhibit significantly different group delays as a result. (This difference is not important in most applications. Some equalizer designs may be better able to cope with poor quality lines, but any two modems using the same scrambler algorithm should be able to communicate with each other in principle.) Since only the sum of the two group-delays is determined by the measurement hardware, the arrival of the on-time marker will be in error by one-half of the difference between the delays in the two directions.

The uncertainties resulting from the 1200 bit/s modems will therefore be composed of three components: one-half of the difference between the scrambler/equalizer delay in the NIST modem and the user's modem, a synchronizer delay at each end with a mean value of 417 μs and a smaller, slowly fluctuating delay resulting from changes in the automatic equalization.

4.3 Delays and Offsets in the Receiver

In order for the NIST hardware to measure the round-trip group delay, the receiver must echo the received message (and particularly the on-time marker). If this is done using a circuit similar to figure 4, for example, the delay between the receipt of the on-time marker and its return to NIST is likely to be stable with a value much smaller than any of the delays discussed above. The delay between the receipt of the on-time marker and the leading edge of the output pulse will also be very small.

If the on-time marker is detected and echoed using software, however, the arrival time of the character is less well defined and may involve both hardware and software delays. The cycle speed of most digital circuits is fast enough so that the sum of these delays is unlikely to be significant in a dedicated single-program environment running with all other interrupts disabled, but is likely to be ill defined in more complex situations.

The arrival of the on-time marker is an asynchronous event with respect to the local clock, and this adds additional complications. We can illustrate these difficulties using a popular type of personal computer. The clock in this type of computer consists of an oscillator with a frequency of 1193180/65536 Hz (about 18.2 ticks/s), and the time is kept as the number of ticks past midnight. It is not possible to read or set the clock to a fraction of a tick. This has two significant consequences:

1. Since there are not an integral number of ticks/s, not all times can exist. For example, 00:00:01.00 is not an integral number of ticks after midnight and therefore can not be set and will never be read. The nearest times are 00:00:00.98 and 00:00:01.04. The average offset between any given time and the nearest time that can be set is 0.5 ticks or about 28 ms.

2. Time intervals are also uncertain by up to 1 tick since the tick fraction when the time is read cannot be known to the program. Again, the average offset is 0.5 ticks (28 ms). This problem increases the uncertainty in measurements of short time intervals and also makes it difficult to estimate the rate of the local clock with respect to NIST using second differences of the local time and UTC(NIST). A typical value for the rate offset of a clock in a small computer is about 1 s/d. Consecutive calibrations of this clock must be separated by at least 10 h if this rate is to be estimated with an uncertainty of no more than 10% using second differences between the local time and UTC(NIST).

If the cycle-speed of the hardware is known, it is possible to interpolate between ticks using short loops to measure the time between the arrival of the on-time marker and the next tick of the local clock in units of the cycle speed of the processor, but this strategy is only useful in a single-user environment when other interrupts are disabled. This capability is incorporated into the latest version of the NIST software for personal computers.

4.4 Delays and Offsets in the Transmitter

There are two critical timing operations that are performed by the transmitting hardware: the measurement of the round-trip transit time of the on-time marker, which is used to determine the advance for subsequent transmissions, and the advance itself.

The round-trip transit time is measured by a counter that is started when the on-time marker is sent to the output port for transmission and is stopped when the software recognizes that the appropriate character has just been received. The resolution of the counter is 200 ns. The frequency used to drive the counter is derived from a cesium standard and the uncertainty of this measurement is very small compared to the other effects that have already been discussed.

The uncertainty in the advance is also negligible compared to the other effects. The advance is determined modulo 10 ms using a 100 Hz signal

derived from a cesium standard and synchronized to be coincident with UTC(NIST); the remainder is determined using a signal derived from a local 6 MHz crystal oscillator that is also used as the clock for the processor chip that controls the system. This frequency need not have high accuracy since it is used only to measure a small time interval.

4.5 Transmission Errors

Transmission errors are usually caused by broadband noise on the telephone line, by echoes, or by cross-talk interference from another telephone circuit. The error rate is too small to estimate accurately, but is unlikely to exceed 10^{-6} unless the telephone connection is unusually noisy.

Since the probability of an error within a single transmission is quite small, NIST transmissions do not contain checksums or other provision for error correction. Successive transmissions are highly redundant, however, and error detection can be included in the design of the receiver without much difficulty. There are several different possibilities to consider, depending on where the error occurs.

1. The on-time marker (* or #) is garbled or lost. If an output pulse was to be generated on receipt of the on-time marker, then no pulse will be sent, and the interval between two consecutive on-time markers will be too long by 1 s. If the on-time marker was to trigger some process (such as setting the local clock), then that process will not be initiated. The loss of the on-time marker can be detected, since its approximate arrival time is known from previous transmissions. A character received at approximately the correct time could be taken as the on-time marker, but neither the hardware nor the software designed by NIST operates in this way.

2. A transmission error converts another character on the line to the on-time marker (* or #). An output pulse will be generated at the wrong time, and this spurious character will be echoed back to NIST too soon so that the measurement of the delay by NIST will be affected. This type of error could be detected by parsing the complete transmitted line and rejecting an on-time marker if it does not occur in the proper context, but neither the hardware nor the software designed by NIST perform this check.

3. An error occurs in one of the digits of the time. If the error transforms the digit into another character that is not legal in context, it is easily detected since the parsing algorithm will fail. If the character in error is still legal in context, the error cannot be detected by examining the line alone. Since the time is composed of about 12 digits and there are 10 legal digits out of 128 possible codes, the probability that an error will transform a digit of the time into another character that is legal in context is less than 10^{-6}.

The probability that an error of this kind will result in the time being set incorrectly has been minimized in the NIST software by insisting that the times of two consecutive transmissions differ by exactly 1 s. A general version of such a scheme is quite complex since it must cope with all of the peculiarities of the calendar, and only a simplified version has been implemented. The seconds value from the first line of the pair is decoded and examined. If it is greater than 57, then the comparison is postponed, since the following second may be the first second of a new minute. (Second number 58 is the last second of the current minute if a negative leap-second is imminent, second number 59 is usually the last second of the current minute and second number 60 will be the last second if a positive leap-second is imminent.) If the current second is less than 57, the seconds digits are converted to blanks and the remainder of the date and time are stored in a buffer as received. When the next line is received, the seconds value is extracted and tested for equality with the previous value +1. If this comparison succeeds, the remaining digits of the date and time (with the seconds field converted to blanks in both cases) are compared character by character (all characters must be the same). If either comparison fails a transmission error is assumed, and the process is begun again with the next two lines since the program has no way of knowing which of the two lines is in error. This process continues until two consecutive lines are decoded and are found to be consecutive or until the NIST hardware hangs up the telephone.

This method will detect almost all of the errors that could not be detected by any of the previous methods; it reduces the probability that the time will be set incorrectly to less than 10^{-12}.

4.6 Results of System Tests

We have evaluated the performance of the ACTS system using both satellite and ground-based telephone circuits. The satellite test was performed between the NIST radio station WWVH in Hawaii and our laboratory in Boulder, Colorado; the ground-based test used a local telephone call in Boulder.

In both tests, we dial the NIST ACTS telephone number, establish a telephone connection, echo all characters back to the transmitter and wait 6 s for the time-delay measurement to stabilize. We use either the circuit of figure 4 or a personal computer running our software to produce a pulse each time the on-time marker arrives at the receiver. We measure the time differences between these pulses and the ticks of a local time standard. These tests are repeated at different times of the day and using different brands of modems, all of which conform to the appropriate standard.

Consecutive measurements over both the satellite and local telephone connections showed a repeatability of ± 1 ms at both 300 and 1200 bits/s. This specification is most important for time-interval measurements or frequency calibrations. It is consistent with the value to be expected from the previous discussion, and suggests that both satellite and local telephone connections are reciprocal to a very high degree.

The accuracy of the arrival time of the on-time marker was measured using several different brands of modems. All of the tests used local telephone connections. At 300 bits/s, the offset of the on-time marker was not more than ± 2 ms for any modem tested. At 1200 bits/s, different brands of modems resulted in offsets of up to ± 7 ms. These values are significantly larger than the repeatability using any one modem, and result from the difference in the group delay between the transmit and receive portions of the modem as discussed above.

The accuracy of the satellite connection to Hawaii was measured using a single modem at both speeds. We measured an accuracy of 1 ms using 300 bits/s and 6 ms using the 1200 bit/s protocol. These values were stable from day to day to within the repeatability quoted above, and suggest that the satellite path is also reciprocal to a very high degree.

5. Applications

One of the most important applications for ACTS is the maintenance of accurate time within a digital computer or some digital hardware with a microprocessor. This might be required, for example, for tagging of business transactions or scientific data. Where a number of computers independently tag events with the date and time and then share their information, it may be especially important to know that the clocks in all of the computers are set to the same time.

A second application is the measurement of frequency. Here pulses coincident with the OTM are used to start and then stop a counter which counts the output of the oscillator under test. If the start and the stop pulses are separated by one day, then the system can yield a frequency-measurement accuracy of about one part in 10^8.

6. Discussion and Conclusions

NIST is now committed to long-term operation of a new Automated Computer Time Service. The format is now fixed, except for a change which will modify the 300 bit/s format to transmit the entire time/date message every 2 s. The system will be expanded as the number of calls increases. The telephone number for the service is (303) 494-4774. All of the lines will be connected to a telephone rotary switch so that they can be reached by dialing this number. This number is not toll-free and might be changed in the future.

The system was designed to make operation at the user's end particularly simple. With telephone-line delay measured at the NIST end, the user needs only a modem and a computer or some other digital system to access NIST time at accuracies of up to 1 ms. Example software and hardware has been developed by NIST, and the software is available for a small charge.

The system can be used to set digital clocks, or to perform frequency calibration at an accuracy of one part in 10^8 for a one day measurement. For systems that are already connected to the telephone line, little effort is needed for setting time. We might imagine development of a number of products which could take advantage of this. For example, a digital clock and microprocessor built into a telephone receiver could provide for a clock which is "always right." Such a telephone could be designed to distribute time to other clocks within a business, school or factory. Automated calling could be done during night hours when the telephone charges are least expensive. If this approach is used, we ask that some effort be directed toward spreading the calling times out over a broad period so that the ACTS system is not heavily taxed in some narrow time frame (e.g., midnight).

The uncertainties in the method are fully discussed in section 4. Using a transmission speed of 1200 bits/s, the major systematic offset is the asymmetry in the delays of the pair of modems. This offset is largely removed at 300 bits/s. At either speed, the path between the receiver and the trans-

mitter contains several asynchronous to synchronous conversions. The jitter inherent in such processes is the largest single contributor to the error budget; it cannot be removed using the current components.

These uncertainties result from the use of standard modems and protocols which were chosen to make the system widely available and simple to use; more specialized, higher accuracy versions of the protocol, using special-purpose hardware, are under consideration. The ultimate limitation of the method is the lack of perfect reciprocity in the telephone connection. Preliminary measurements suggest that the group delay in a local telephone loop is stable and reciprocal to about 20 μs, suggesting that both the repeatability and the bias might be improved by a factor of 50 using appropriate transmission hardware.

About the authors: *D. B. Sullivan, a physicist, is the Chief of the Time and Frequency Division in the National Measurement Laboratory; the other authors are staff members in that Division, which is located at NIST, Boulder, CO. J. Levine, M. Weiss, and D. W. Allan are also physicists while D. Davis is an electronics engineer.*

Volume 94, Number 5, September-October 1989
Journal of Research of the National Institute of Standards and Technology

Errata

Erratum: Scattering Parameters Representing Imperfections in Precision Coaxial Air Lines

Donald R. Holt

National Institute of Standards
and Technology,
Boulder, CO 80303

[J. Res. Natl. Inst. Stand. Technol., Volume 94, Number 2, March-April 1989, p. 117]

The following errors were found in this paper:
On page 121, eq (2.7b) should read:

$$\frac{\mathrm{d}A_{\bar{0}\bar{0}}}{\mathrm{d}z} - j\beta A_{\bar{0}\bar{0}} = -\frac{1}{2}\frac{1}{\ln\dfrac{b(z)}{a(z)}}\left\{\frac{b'(z)}{b(z)} - \frac{a'(z)}{a(z)}\right\} A_{\bar{0}\bar{0}}^{+}.$$

On page 121, the equation immediately above eq (3.2c) should read as follows:

$$C_{k-1}(0) = \hat{C}_{k-1}(z_{k-1}).$$

On page 121, the sentence immediately below eq (3.2c) should read:

such that $C_{0,k-1}$ represents the measurement of $a(z)$ or $b(z)$ at $z = z_{k-1}$.

On page 122, eq (3.8) should read:

$$A_{\bar{0}\bar{0}}(0;z) = A_{\bar{0}\bar{0}}(0;z_1) - A_{\bar{0}\bar{0}}^{+}(0;z_1)\{e^{-j\beta z_1}\int^{z-z_1} \ldots \quad .$$

On page 129, the sentence immediately below eq (A.11) should read:

Substituting $E_r = \tan\{\phi_a(z)\}\, E_z \ldots$.

On page 133, eq (D.3) should read:

$$\ell_0 = \sum_{n=0}^{N-1} \ldots \quad .$$

Volume 94, Number 5, September–October 1989
Journal of Research of the National Institute of Standards and Technology

Conference Reports

NINTH CONFERENCE ON ROOFING TECHNOLOGY
National Institute of Standards and Technology, May 4–5, 1989

Report prepared by

Walter J. Rossiter, Jr.

Building Materials Division,
Center for Building Technology,
National Institute of Standards and Technology,
Gaithersburg, MD 20899

The National Institute of Standards and Technology (NIST) Center for Building Technology (CBT) and the National Roofing Contractors Association (NRCA) have joined in sponsoring Conferences on Roofing Technology on a biennial basis since 1969. In 1977, NIST and NRCA co-sponsored the First International Symposium on Roofing Technology, and in 1985, they were joined by RILEM[1] in co-sponsoring the Second International Symposium on Roofing Technology. These Conferences are the major industry forum for the discussion and dissemination of research results and the presentation of the latest advances in roofing technology. Papers in the Conferences and Symposia address roof performance from fundamental and practical viewpoints.

1. The Conference

The theme of the 1989 Conference was "Putting Roofing Technology to Work." This was appropriate considering the general challenge facing U.S. industry to use our strong scientific and technological capability for making the Nation more competitive in international markets and to build strong links between the base of scientific knowledge and the transfer of knowledge to practice.

Approximately 380 individuals were in attendance. They represented a broad spectrum of the roofing community including architects, engineers, consultants, contractors, specifiers, researchers, and building owners. Fourteen invited papers were presented in a format that included an introductory session and three technical sessions entitled Maintenance, Insulation and Vapor Retarders, and Membranes. An extended question and answer period followed each of the technical sessions with the speakers responding to written questions submitted by the audience and asked by the session chairperson. A Proceedings was published and is available from the NRCA.[2]

2. Introductory Session

In this session, William Cullen, formerly of NIST, presented a paper [1] entitled "Transitions in Roofing Technology," which set the theme for the subsequent presentations. Cullen reviewed the

[1] Reunion Internationale des Laboratoires d'Essais et de Recherches sur les Materiaux et les Constructions.

[2] One O'Hare Centre, 6250 River Road, Rosemont, IL 60018; telephone 312-318-6722.

major milestones that the roofing industry has experienced over the last century. His emphasis was on the lessons that have been learned in using technology to solve specific problems. He reminded the audience that technological advances are not always without penalty. He gave several examples where solutions to problems have, at the same time, created new problems that also required technical remedies. He discussed in some detail the advances that have occurred over the last two decades in applying measurement-related technologies to improving roofing performance. His closing comments indicated that, although significant advances have been made, much remains to be done. For example, the application of simulation modeling and use of expert systems are in their infancy in the industry.

3. Session on Maintenance

The first two papers [2,3] in the session focused on planned maintenance for extending the life of existing roofing systems, and setting priorities for conducting maintenance activities in cases where a number of roofs are under the responsibility of a single building owner. Owners have considerable investments in roofs, and sound maintenance programs are a means of protecting the investments. The U.S. Army Construction Engineering Research Laboratory (CERL) has developed a systematic approach for assessing the maintenance needs for built-up roofing systems on Army facilities. It is a computerized methodology, called "ROOFER," that provides an assessment of the condition of a roof based on visual observations from an on-site inspection and tests conducted to determine the amount of moisture in thermal insulation. ROOFER will provide building managers with a procedure for identifying roof problems, and for making practical decisions in setting maintenance and repair strategies and priorities. The program and users' manuals are expected to be available later in 1989.

The third paper [4] in the session described the U.S. Air Force's philosophy in obtaining maintainable roofing systems. The requirements consider all parties involved in the service cycle of the roof and include:

- concentrating on maintainability during the design stage,
- obtaining the best quality systems that are available,
- using trained, qualified installers, and
- commitment by the owner to a rigorous maintenance program.

The paper emphasized the last parameter as an item often overlooked by myopic owners who ignore their roles in maintaining roofs. It was pointed out that owners should not expect satisfactory long-term performance from their roofs unless they are willing to invest in a maintenance program.

In concluding the session [5], the latest developments in roof coatings were described. The application of coatings to the surfaces of existing roofs is a maintenance technique that may be used for increasing the longevity of some types of roofing systems. The topics addressed in the paper included a review of the types of coatings available, their uses, advantages, and limitations.

4. Session on Insulation and Vapor Retarders

A key parameter affecting the performance of low-sloped roofing systems is the compatibility of the insulation and the membrane. A paper [6] on this subject gave many examples of problems that have arisen when the designer has ignored compatibility. It was pointed out that a database on the performance requirements of insulation/membrane systems has not been developed by the industry. Such a database is needed to establish compatibility requirements.

The U.S. Army Cold Regions Research and Engineering Laboratory (CRREL) has been studying the needs for vapor retarders in low-sloped roofs for many years. The second paper [7] in the session summarized the results of the studies. Maps and graphs that may be used to determine when and where vapor retarders should be installed were presented. The author emphasized the importance of air leakage as a primary mechanism behind condensation problems in buildings, and recommended that the first defense against condensation in low-sloped roofs is to control air leakage into the system.

A major item of concern facing the industry in recent years has been the wind resistance of mechanically fastened single-ply systems. In these systems, the fasteners are normally located in the membrane seams and are driven through insulation boards and attached to the structural deck. Experience has shown that some of these systems have performed less than satisfactorily due to severe wind exposure. Factors affecting their performance

are not completely understood. A paper [8] was presented describing the results of tests conducted using a fatigue device developed to simulate wind-uplift conditions. Variables in the testing included the membrane, type and density of insulation, and the type of fastener system and seam. Based on the results of the study, a number of practical recommendations were provided for improving the performance of mechanically fastened systems on exposure to severe wind cycling.

The final paper [9] in the session described the results of an initial experiment on thermal performance using the recently constructed large-scale climate simulator (LSCS) at the Oak Ridge National Laboratory (ORNL). The LSCS provides for thermal measurements of roofing sections subjected to a wide variety of external and internal environments. In the experiment, the thermal resistances of three common insulation boards were measured over an extended range of temperatures using two different techniques, one steady state and the other transient. Results from the two techniques were in agreement with one another and within 5% of reference values published for the test specimens. The initial experiment demonstrated the successful use of the LSCS, thus setting the stage for much needed future research on the thermal performance of low-sloped systems.

5. Session on Membranes

The lead paper [10] in this session addressed the application of thermal analysis techniques such as thermogravimetric, dynamic mechanical, and torsion pendulum analyses to the characterization of roof membranes upon aging. A unique aspect of this paper was its co-presentation by an American and a Swiss. The authors had co-chaired a task group under the auspices of the Joint CIB[3]/RILEM International Committee on Elastomeric, Thermoplastic, and Modified Bituminous Roofing. The paper was a synopsis of their task group's work. In introducing their subject, the authors reminded their audience that the thermal analysis techniques have been long available in many areas of science and technology, but have had little use in assessing roofing membranes, in spite of the sensitivity and reproducibility of the methods. As examples of the utility of the techniques, they presented data taken of rubber, thermoplastic, and polymer-modified bituminous materials before and after exposure to either natural or artificial environments. They concluded by recommending that the use of the methods be refined and standardized specifically for application to roofing membrane materials.

Two papers [11, 13] in the session from NIST addressed the effect of surface contaminants on the strength of adhesive-bonded joints in EPDM single-ply roofing membranes. The first was a laboratory evaluation whereby a known quantity of talc was deposited on cleaned EPDM rubber, and contaminated joint specimens were subsequently prepared. The quantification of the amount of talc involved the use of a computer image analysis method, developed specifically for the study, that was based on the reflectance of light from the "talc-ed" rubber surface. As the amount of talc increased, the surface reflectance of the sheet also increased. The results of the study showed that, for the contaminated T-peel joint specimens, their strength after cure times greater than 2h was highly dependent on the contamination level. The maximum strengths were achieved with specimens that were thoroughly cleaned. In a related NIST field study, strength data were presented for EPDM joint specimens taken from roofs in service. It was found that their strengths were low in comparison to values obtained from control specimens fabricated in the laboratory using cleaned rubber. Scanning electron microscopy of the rubber surfaces of the field specimens showed the presence of talc-like particles that could have contributed to the observed low strengths.

Another paper [12] on membranes discussed the field application of polymer-modified bituminous membranes. The use of these materials has increased substantially in the last few years, and now accounts for about 18% of the current membrane market. The author of the paper reviewed concerns that the industry faces to assure their proper application. Chief among them is the adhesion of the membrane sheets to the roof, as well as to themselves, to form watertight seams. Current adhesion techniques involve thermal methods whereby either heat is applied directly to the sheet to soften the bitumen for bonding, or hot asphalt is used as a bonding agent. Consequently, adequate temperature control under the variety of weather conditions encountered during field application is necessary for proper bonding. To overcome the limitations imposed by the need for precise temperature control, the use of cold-process adhesives for bonding sheets and seams is expected to increase in the future.

[3] A French acronym indicating the Conseil Internationale due Batiment pour la Recherche, l'Etude, et la Documentation.

The final paper [14] of the Conference was a review of the advances in built-up roofing technology made over the last one and one half decades. Significant developments have occurred such as the development of membrane performance criteria and viscosity-related criteria for asphalt application. The author of the paper expects continued advances with the introduction of new reinforcing fabrics, and polymer-modified asphalts. Reliable techniques for assessing long-term performance will have to be developed to facilitate acceptance of new materials and practices.

6. Summary

The papers presented by the authors described problems and concerns that have confronted the roofing industry in recent years. Recommendations were presented for alleviating these problems and providing improvements in roof performance. Nevertheless, in many papers, the authors noted that much remains to be accomplished through research and technology for the continued betterment of the industry. From the perspective of a NIST attendee, it was clear that measurement-related advances in the industry are needed to assist in "putting technology to work," as the theme of the Conference urged. As examples, the development of methods for assessing long-term performance of new materials, the application of nondestructive techniques for evaluating existing systems and components, and the development of reliable methods for assuring the quality of systems that are fabricated in the field are noted.

7. Bibliography of Conference Papers

[1] Cullen, W. C., Transitions in Roofing Technology.
[2] Bailey, D. M., Brotherson, D. E., and Tobiasson, W., ROOFER: A Management Tool for Maintaining Built-Up Roofs.
[3] Bradford, J., Planned Maintenance for Commercial Roofing.
[4] Firman, D., Maintenance Needs: An Owner's Perspective.
[5] Brzozowski, K., New Coatings as Components of Roofing Systems.
[6] Van Wagoner, J. D., Compatibility of Roofing Insulations and Membranes.
[7] Tobiasson, W., Vapor Retarders for Membrane Roofing Systems.
[8] Murphy, C., Lap Attachment of Mechanically Fastened Roof Membrane Systems.
[9] Courville, G. E., Shipp, P. H., Petrie, T. W., and Childs, P. W., Comparison of the Dynamic Thermal Performance of Insulated Roofing Systems.
[10] Backenstow, D. and Flueler, P., Thermal Analysis for Characterization.
[11] Martin, J. W., Embree, E., and Rossiter, W. J., Jr., Effect of Contamination Level on Strength of Butyl-Adhered EPDM Joints in EPDM Single-Ply Roofing Membranes.
[12] DuPuis, R. M., Concerns in The Application of Modified Bitumen.
[13] Rossiter, W. J., Jr., Seiler, J. F., Jr., and Stutzman, P. E., Field Testing of Adhesive-Bonded Seams of Rubber Roofing Membranes.
[14] Baxter, R. P., Developments in Built-Up Roofing 1978-1988.

Volume 94, Number 5, September–October 1989
Journal of Research of the National Institute of Standards and Technology

News Briefs

General Developments

SEVENTH INTERNATIONAL TEMPERATURE SYMPOSIUM PLANNED

A symposium on Temperature, Its Measurement and Control in Science and Industry will be held in Toronto, Ontario, in April 1992. The symposium, seventh in the series that began in 1919, will provide a showcase for the major advances in thermometry since the Sixth Symposium in 1982. The symposium will take place in the Toronto Convention Center, in conjunction with the semi-annual exposition of the Instrument Society of America. Sponsors for the symposium include NIST, the American Institute of Physics, the Instrument Society of America, and the National Research Council of Canada. The General Committee that is planning the symposium is headed by Lawrence G. Rubin of the Francis Bitter National Magnet Laboratory at the Massachusetts Institute of Technology. James F. Schooley of NIST is the chairman of the program committee. It is expected that the Proceedings of the Seventh Temperature Symposium, like those of earlier meetings, will become a primary reference for the field of thermometry.

LESL STANDARD FOR FM RECEIVERS WILL ASSIST LAW ENFORCEMENT AGENCIES

The National Institute of Justice (NIJ) recently published NIJ Standard-0206.01, Fixed and Base Station Receivers. This publication is based on NIST research and is a revision of a standard published in September 1975. It includes requirements and test methods for units operating in the 800-MHz frequency band. In addition, it provides updated requirements for receiver sensitivity, closing time, and audio response and describes modified tests for spurious and harmonic response and intermodulation attenuation. Thirteen different tests are specified by the standard.

PRECISION SOURCE OF CALCULABLE DIGITALLY SYNTHESIZED AC VOLTAGES MADE AVAILABLE

In response to industry needs, NIST scientists have developed a reference digitally synthesized source (DSS) of ac voltages. These sources are capable of serving as transfer standards at the 3-7 V level with accuracies of 10-20 ppm from 10 Hz to 10 kHz, and even greater accuracies below 10 Hz. The significance of the DSS is that the rms value of its stepped output waveform can be calculated, based on accurate dc voltage measurements.

Applications have demonstrated that the DSS constitutes an effective overall reference that takes into account losses due to connectors, cables, switches, and other sources of error in a complete ac voltage measurement instrument or system. It has been used to verify the performance of the ac measurement section of a new multimeter having a claimed accuracy of 100 ppm.

The division is prepared to loan the developmental DSS on a trial basis to organizations that have the metrology capability to use it effectively. Division staff have described the DSS at the Conference on Precision Electromagnetic Measurements, at two other major conferences, and in a paper to appear in the *IEEE Transactions on Instrumentation and Measurements*.

DEPARTMENT OF AGRICULTURE TO ADOPT NIST HANDBOOKS

The U.S. Department of Agriculture (USDA), Food Safety and Inspection Service, has published a proposal in the *Federal Register* to incorporate by reference, *Checking the Net Contents of Packaged*

Goods (NIST Handbook 133,) and *Specifications, Tolerances, and other Technical Requirements for Weighing and Measuring Devices* (NIST Handbook 44) into their regulations.

Incorporation will bring federal and state regulations into conformity. Since 1984, USDA, the Food and Drug Administration, and representatives of consumers and the meat and poultry industries have been working through the NIST-sponsored National Conference on Weights and Measures (NCWM) to resolve the net weight issue.

The proposal contains the agreements worked out by the interested parties through the NCWM. It will amend the federal meat and poultry products inspection regulations to provide uniform net weight labeling requirements, including reasonable variations for label statements of net contents of meat and poultry products.

In the notice, the USDA states that "The National Conference on Weights and Measures has become the principal forum for building a consensus on how to determine the net weight of meat and poultry products."

SELF-LUBRICATING COMPOSITES STUDIED FOR WEAR AND FRICTION PROPERTIES

Ceramic-matrix and metal-matrix composites are being prepared and studied in sliding wear in the tribology group of the Ceramics Division. The composite materials include a soft, solid lubricant phase, $NiCl_2$ intercalated graphite. During wear of the composite, some of the soft phase is retained in the sliding contact to maintain an effective solid lubricating film. Matrix materials being studied include alumina, silicon nitride, and copper. The composites were slid against hardened steel.

Friction coefficients in sliding were reduced by factors up to 4 (copper 0.6 to 0.15, silicon nitride 0.45 to 0.17) by this approach. Wear rates were also significantly reduced. Studies of the worn surface morphology showed three significant mechanisms at work: (1) the formation of a lubricating interfacial film from the exit boundary of the soft phase regions; (2) recession from the average surface height at the soft phase regions; and (3) collection of wear debris in the recess at the entrance region of the soft phase. Further understanding of these and other mechanisms that control wear and friction should permit alteration of composite composition and microstructure to further improve the tribological properties. Self-lubricating composites can be used in applications where liquid lubricants cannot be used to control friction and wear. A patent disclosure concerned with the composite fabrication methods that were developed in the project, has been submitted.

NIST-INDUSTRY COLLABORATION ON AN ADVANCED COMPOSITE MATERIAL

Graphite-epoxy composite rods are being considered as tethers for a new type of offshore oil platform called the TLP, or tension leg platform. The tethers connect the floating platform to the seabed. For tethers 1 km or more in length, the mass of conventional steel tethers becomes a significant consideration in the design. Unidirectional graphite-epoxy offers the possibility of tethers of only one-sixth the mass of steel tethers for equivalent strength.

Because advanced composite materials have no service history on offshore oil platforms, designers are reluctant to use them to replace steel. At a meeting to explore NIST-industry collaboration, it was suggested that optical fibers could be embedded in the fibers to provide warning of damage. The availability of diagnostic information on the condition of the composite tethers could compensate for lack of experience with these materials.

The result was the tether prototypes with embedded optical fibers have been produced cooperatively by industry and samples have been supplied to NIST. Preliminary tests have verified the high strength and stiffness of the rod, and that the optical fiber survived the manufacturing process intact. Experiments to explore the correlation between changes in the optical behavior of the embedded fiber and mechanical loading and damage on the rod are under way.

A NOVEL DILATOMETER FOR POLYMER STUDIES

A high-precision torsional dilatometer has been constructed in the Polymers Division to study the effects of deformations on the physical aging and rejuvenation of polymeric glasses. The instrument is fully automated with the capability of simultaneously measuring the torque, normal force, angular displacement, temperature, and volume change of a polymeric glass subjected to torsional deformations.

The volume of a polymeric glass contracts spontaneously toward the equilibrium value in a slow process referred to as physical aging. These small volume changes cause large changes in the mechanical properties, which makes the rate and extent of physical aging of practical importance. On

the other hand, the mechanical stimulus of deformation has been postulated to cause changes in the structure (volume) of the glass and therefore bring about rejuvenation. Because the magnitude of the relative volume changes required to cause rejuvenation are of the order of 10^{-3}, experiments such as tension or compression, which cause large (of the order of 5×10^{-3}) volume changes, cannot be used to test the hypothesis.

Preliminary measurements performed on epoxy glasses aged into equilibrium show that torsional deformations induce an increase in relative volume of the order of 1×10^{-4} to 1×10^{-3}. The volume increase scales approximately as the square of the deformation and the kinetics of the volume recovery after the deformation differ from the relaxation kinetics of the torque and normal force. These results are unexpected and, if confirmed, will lead to renewed interest in theories of physical aging of glasses.

The low machine compliance and 5 mK temperature stability of the torsional dilatometer make possible relative volume change measurements of $1\times10^{-5}\pm10^{-7}$ to be made over time periods in excess of several hours. Volume change measurements at times as short as 10^{-3} s are possible, although the system mechanics currently limit the practical measurement range in isothermal experiments to approximately 0.1 s. The temperature stability of the dilatometer and the ability to study short time phenomena will be exploited in the future to study the effects of deformations on the phase behavior and kinetics of phase separation of two-phase polymer systems near the critical point.

MAGNETIC MEASUREMENTS OF SINGLE-CRYSTAL HIGH-TEMPERATURE SUPERCONDUCTORS

Single crystals of $YBa_2Cu_3O_{7-x}$ (YBCO) have many properties of great interest for the development and application of high-temperature superconductors. For example, when fully oxygenated ($x=0$), such crystals have very sharp transitions to the superconducting state and the highest critical currents reported for any of the new superconductors. High-quality crystals with dimensions up to $0.3\times0.3\times0.2$ mm have been grown. These crystals, having volumes on the order of a few millionths of a cubic centimeter, make the characterization of their superconducting properties a difficult task. However, NIST scientists have been able to characterize them using the high-measurement sensitivity available with a Superconducting Quantum Interference Device (SQUID). As with all YBCO material studied to date, the as-grown single crystals are not perfect, but are highly twinned. Perfect untwinned crystals will allow anisotropy to be fully characterized, the role of twins to be determined, and theories concerning the role of oxygen chains to be investigated. Therefore, the current goal of this effort is to produce perfect, untwinned, and fully oxygenated single crystals and to charac terize their properties in all three directions. Single crystals, which are more than 99 percent twin-free, have been produced. The first magnetic moment measurements on untwinned crystals have been accomplished. Further work is in progress in order to fully oxygenate and maintain a twin-free state.

NIST SCIENTISTS PROVIDE RADIATION DATA FOR INTERNATIONAL REPORT ON TISSUE SUBSTITUTES

A new authoritative report, *Tissue Substitutes in Radiation Dosimetry and Measurement,* Report 44 (1989) of the International Commission on Radiation Units and Measurements (ICRU) includes radiation interaction data that, for the most part, was provided by Ionizing Radiation Division scientists at NIST. The report is important because of the need to measure absorbed doses on both macroscopic and microscopic scales within and around irradiated body tissues. These measurements require the use of carefully selected materials from which radiation detectors and phantoms (substitutes for portions of the body) are constructed. The 133-page radiation interaction data table includes photoelectric, coherent, Compton and pair production cross sections, mass attenuation coefficients, mass energy absorption coefficients, electron stopping powers, proton stopping powers, and neutron kerma factors. Data are given for 24 actual tissues, plus 53 solid and liquid tissue substitutes and 10 gaseous tissue substitutes.

DOUBLE-AMPLIFICATION FLOW-INJECTION IMMUNOASSAY DEVELOPED AT NIST

Analyses based on immunological (antigen-antibody) recognition have, because of their high specificity, become one of the most widely used techniques in the clinical laboratory. When combined with radioactive, fluorescent, or enzyme tags, these immunoassay techniques are also among the most sensitive. At NIST, scientists have developed an even more sensitive, and quantitative,

immunoassay based on a regenerable, computer-controlled flow-injection system incorporating a novel double-amplification approach.

The double amplification is achieved by means of peroxidase enzyme molecules encapsulated in analyte-derivatized liposomes. The enzyme is released subsequent to a competitive immunological reaction between analyte molecules (theophylline, a drug used for treating asthma) and immobilized antibodies. The released peroxidase enzymatically cleaves, from an organofluorine substrate, fluoride ions which are then potentiometrically measured. By means of immunoreactor column regeneration and calibration, accurate quantitation can be achieved; a feature missing from conventional batch-type immunoassays.

By this liposome/enzyme double-amplification approach, theophylline was determined over a range of concentrations from 0.2 to 4000 ng/mL. The detection limit of 200 pg/mL corresponds to about 100 fmol (10^{-15} mol) of theophylline measured in the 100 μL sample injected. The system is currently undergoing further development to optimize its operating characteristics.

ULTRAFAST ENERGY TRANSFER AT SURFACES

Ultrafast lasers have been used at NIST to measure the vibrational population relaxation time, T_1, for small molecules bound to platinum or rhodium particles, typical materials used as catalysts. These experiments provide the first direct evidence for the role of substrate electronic states in transferring energy initially localized in specific molecular bonds. The results suggest that vibrationally excited adsorbed molecules may play a more important role in laser-controlled surface chemistry than had previously been anticipated.

Specifically, a stretching vibration in carbon monoxide, CO, bound to Pt or Rh was strongly excited by a resonant picosecond (1 ps$=10^{-12}$ s) laser pulse. The subsequent decay of the CO($v=1$) population was then detected by the transient change in absorption of a weak, time-delayed ps probe pulse at the same frequency. The decay time for CO on these particles, which consisted of about 1,000 metal atoms, was found to be $T_1=7$ ps, one to two orders of magnitude shorter than that in small metal carbonyl molecules. The dramatic increase in relaxation rate suggests that the metal particles provide a new and rapid pathway for the decay of energetic surface species.

The exceptional ability of metal surfaces for increasing molecular relaxation rates beyond those found in solution or on insulator surfaces had previously been predicted. However, the observed increase is still a factor of 10 less than predictions based on indirect evidence such as spectral linewidths.

TIME- AND STATE-RESOLVED STUDIES OF MOLECULAR DECOMPOSITION

Experiments performed with pump-probe, picosecond laser techniques have now produced new insights into the nature of molecules that contain sufficient vibrational energy to decompose. The experiments indicate that molecular product states and appearance rates are highly dependent upon the initial vibrational motion and energy. For example, two vibrational states of HN_3 with nearly identical energies exhibit dissociation lifetimes different by a factor of 2.

The unprecedented scope of these measurements makes HN_3 a benchmark system in our understanding of unimolecular decomposition. The observations of state mixing and mode-specific decay have profound implications for laser-selective chemistry.

NCSL TO TEST INTEROPERABILITY OF OSI X.500 DIRECTORY SERVICES

National Computer Systems Laboratory and other participants in OSINET begin interoperability testing for the Open Systems Interconnection (OSI) X.500 Directory Services this year. OSINET is a network established by NCSL to test and demonstrate the OSI protocols. The X.500 standards provide a directory database of all devices or users on a network. The directory access protocol within X.500 provides a way for naming and addressing devices on a network and a way to have multiple directories exchange information so messages can be routed around networks. Vendors and users participating in the project will test the various implementations of the X.500 protocol.

NIST DEVELOPS NEW FABRICATION METHODS FOR FIBER CURRENT SENSORS

NIST scientists have developed repeatable fabrication methods, involving the use of special forms, for fiber current-sensor coils; coils of about 200 turns and 1 cm in diameter have been made. Polarization effects in single-mode fiber, primarily stress-induced birefringence resulting from bending, have

previously made it impossible to produce fiber current sensors smaller than about 10 cm in diameter or with more than a few turns. Birefringence before annealing one of the new coils is on the order of 7000 degrees (0.6 radians per turn); after annealing, an entire coil will typically have a birefringence of only 10 to 20 degrees (sensor application requires birefringence of less than 50 degrees). The NIST sensors are the smallest and most sensitive fiber current sensors reported to date. NIST scientists believe they have refined the fabrication process, including packaging, to the point that successful commercialization can take place.

CBT COMPLETES THOROUGH ANALYSIS OF THE INDOOR AIR QUALITY IN A NEW GOVERNMENT OFFICE BUILDING

At the request of the General Services Administration, NIST researchers completed an analysis of indoor air quality of a seven-story federal office building in Portland, OR, that was constructed during 1986 and 1987 and has been occupied for the past 18 months. The purpose of this evaluation was to document the effect of various design, construction, and operation parameters on indoor air quality. This evaluation was done using a special diagnostic center on the building's first floor with instrumentation connected to sensors throughout the building. Measurements were made of air infiltration, ventilation rates, building envelope tightness, interzone air movement, and levels of indoor contaminants. The contaminants measured were carbon monoxide, carbon dioxide, respirable particulates, formaldehyde (HCHO), radon, and volatile organic compounds. Results of the study indicated: (1) adequate ventilation under most operating conditions; (2) excessive uncontrolled building air exchange by infiltration; (3) levels of carbon dioxide, HCHO, radon, and respirable particles well within established guidelines; (4) high levels of carbon monoxide in the vicinity of elevator shafts and stairwells coming from the underground garage; and (5) no evidence of significant outgassing of pollutants from building materials and furnishings, but the existence of at least 37 volatile organic compounds which appear related to activities occurring within the building.

CFR DEVELOPS SMOKE TOXICITY SCREENING TEST FOR THE NAVY

NIST researchers have developed a new screening test method for the toxic potency of smoke. The Navy will use this method as part of a hazard analysis to control the potential danger from combustible materials on-board submarines. The new "N-Gas Model Smoke Toxicity Screening Test" builds on research over the past 7 years. The principle behind the method states that the toxicity of fire smoke is due only to a few chemical species. This is in spite of the fact that smokes contain hundreds of compounds. In addition to reduced oxygen, scientists have identified the principal toxicants, CO, CO_2, and HCN, and generated data on their toxicities, individually, and in combination. Compared to current smoke toxicity methods, this approach is faster, less expensive, and significantly reduces the dependence on laboratory animals.

NOVEL BIOASSAY FOR MEASURING TOXICANTS IN ENVIRONMENT

A novel laser-bioassay system developed by a private company has been modified during collaboration with Polymers Division scientists for the rapid detection of toxicants in environmental samples. Ultimately, the bioassay method may provide a simple, rapid method for identification and measurement of bioavailability of toxicants in the environment. The system employs strains of genetically defined bacteria which change their growth rate and morphology in response to bioavailable toxicants in samples. The system also provides evidence for the mode of toxicity, based on differential responses of the strains of bacteria which vary only in their ability to repair DNA damage.

Extension of the technique to organometals has been successfully undertaken at NIST in the past year with the demonstration of differential response of bacterial strains to organotin additives and toxicants used commercially as catalysts, plastics stabilizers, and biocides. Responses of bacteria to microgram levels of organotins were measured and several strains were found to respond differently to various organotin compounds. The goal of the joint research is to compare quantitative bioassay measurements with conventional gas chromatographic methods developed at NIST for ultratrace detection and speciation of organotin compounds in environmental samples. The technique is potentially extendable to measurement of other materials including metals, polymers, biocides, and pharmaceuticals. It also offers prospects for standards for bioavailability of molecules in a variety of matrices.

THIRTEEN DECADE PHOTOCURRENT MEASUREMENTS

A high transfer gain, low-noise amplifier and a silicon photodiode have been combined to measure optical radiant power over 13 orders of magnitude at NIST. Since the impedance of the photodiode must be 10 GΩ, the manufacturer must select individual diodes from batch-processed diodes to satisfy this requirement. The high impedance of the photodiode results in low amplification of amplifier noises and drifts which are of comparable magnitude. The low-voltage amplification allows the device to operate at normal laboratory conditions without the complexity of temperature control. The input $1/f$ noise of the amplifier was equalized to the source resistance noise at this high detector impedance in a bandwidth of 0.01 Hz. In this bandwidth, the best measured short-circuit current limit sensitivity was 0.44 fA, which corresponds to a noise equivalent power of 0.73 fW at the 900 nm peak response.

The detector amplifier package can replace photomultipliers in some applications where low-level optical radiation monitoring is required at slow response. The detector package can exhibit better signal-to-noise ratio in these applications and hence can significantly reduce the time for a sequence of measurements. The silicon detector package also allows an absolute calibration of spectral responsivity of the instrument to be provided in those circumstances where the absolute value of the light flux is of interest. The device has application in a large number of situations where sensitivity or wide dynamic range would be important. These include astronomical observations, night vision, photometry, and optical density measurements.

MODEL DEVELOPED FOR ELECTRON TRANSPORT AT METAL-SEMICONDUCTOR INTERFACES

Metal-semiconductor interfaces with large electron transmission probabilities are necessary for the development of high-speed transistors and faster computers. NIST scientists have developed, in collaboration with private industry, a method for calculating "ballistic" electron transport behavior at atomically abrupt coherent interfaces. This method has been applied to interface structures between silicon and nickel silicide, materials typical of those being investigated for high- transmission properties. A surprising result is that the two interface structures that occur in silicon-nickel silicide (the so-called A and B type interfaces) have transmission properties about a factor of three different. Also important to the overall transmission is the degree of match of the important wavefunctions in the two constituent bulk materials. The results provide a theoretical basis for scientists and engineers who are experimenting with related systems and interfaces in the search for ultimate performance electronic devices.

NIST-DESIGNED CRYOGENIC MICROWAVE NOISE STANDARDS PROVIDED TO INDUSTRY

Three primary standard microwave noise sources have been designed, fabricated, evaluated, and delivered by NIST, as an example of the first cryogenic noise standards based on NIST design principles that have been made available directly to U.S. industry. These sources were designed for use with WR10 (75-110 GHz), WR15 (50-75 GHz), and WR22 (33-50 GHz) waveguide systems; the noise temperature for each is 77 K, the temperature of the liquid-nitrogen cryogen. These horn-type sources are very similar to the cryogenic national standard thermal noise sources previously developed that are now in operation supporting measurement services.

Cryogenic noise source standards offer significant advantages in fabrication, operation, and analysis and control of uncertainties over high-temperature sources used previously at NIST and in widespread use elsewhere. The contractual agreement called for a source accuracy of ±2 percent; NIST was able to deliver sources with uncertainties approximately half this: 1.3 percent for WR10, 1 percent for WR15, and 1 percent for WR22.

A COMPARISON BETWEEN PARTICLE SIZE STANDARDS FROM NIST AND BCR

NIST is developing a series of Standard Reference Materials (SRMs) for particle size covering the range of 0.1 to 100 μm. The SRMs consist of aqueous suspensions of monosize polystyrene microspheres. The Bureau Community Reference (BCR), a standards organization for Western Europe, is developing similar standards covering the range of 2 to 10 μm. SRM 1960 (10 μm "Space Beads") was calibrated at NIST using three unrelated techniques: optical and electron microscopy, and light scattering, giving agreement to 0.01 μm.

Recently a comparison was made between SRM 1960 and BCR 167 (9.6 μm), in which each party measured the mean diameter of a sample of the

other party's Standard Reference Material. The samples were known to be uniform at the 0.1 percent level. The measurements used optical microscopy (center distance finding by NIST and array sizing by BCR) for which the base line was provided by interferometrically calibrated stage micrometers. The found agreement was well within the stated calibration accuracies.

CBT COMPLETES NEW COMPUTER MODEL FOR PREDICTING WATER VAPOR SORPTION AT INTERIOR BUILDING SURFACES

The prediction of latent space cooling loads and interior humidity levels in buildings cannot be predicted to the accuracy of many other energy-related quantities. This is due to moisture sorption at interior surfaces of the structure and furnishings being neglected in state-of-the-art energy analysis programs. This phenomena is particularly important when a building is operated with night ventilation to reduce cooling loads. The relative humidity of night outdoor air, however, is often considerably higher than that of the conditioned indoor air during the daytime. Since the amount of moisture stored in building materials depends directly on relative humidity, a significant incremental moisture adsorption occurs during night ventilation with a corresponding desorption during the daytime. Researchers have now completed the development and experimental verification of algorithms that predict moisture sorption rates at interior building surfaces. The model accounts for all surface phenomena including the effect of surface coatings such as paints. This research project involved measuring the basic properties for common materials such as wood and gypsum board. Desorption experiments were then completed with the various materials in desiccator chambers and excellent agreement was obtained between measured and predicted drying rates.

CBT DEVELOPS NEW COMPUTER MODEL FOR REFRIGERANT EVAPORATORS

In order to develop meaningful testing and rating procedures for refrigeration systems that are assembled in the field and cannot be laboratory tested as a complete system, sophisticated simulation tools are required to test components and/or estimate their performance. One such tool just developed by NIST is the computer program EVSIM for modeling refrigerant-to-air heat exchangers used exclusively in residential air-conditioning as an evaporator. The model accounts for any specified air distribution pattern entering the heat-exchanger and a wide variety of refrigerant circuit patterns within the tubes. The model uses a detailed tube-by-tube thermodynamic and heat transfer calculation scheme, and is best suited for mini- and main-frame computers. However, it has been successfully used on an IBM AT-compatible machine. EVSIM has been distributed to leading air-conditioning manufacturers for their use.

USE "ZIP" TO FIND MOST ECONOMIC LEVELS OF INSULATION

How much insulation should be installed in a house? A new computer program called ZIP can help find the answer. Quick and easy to use, ZIP can provide customized estimates of the most economic levels of thermal insulation for building components such as attics, walls, floors, crawlspaces, and basements. ZIP determines these estimates by searching internal data files containing local weather information and energy and insulation costs all keyed to the user's postal ZIP code. The program and supporting files are contained on a single diskette and will run on MS-DOS systems with 256 K of RAM. ZIP was designed by NIST in conjunction with the Department of Energy's Oak Ridge National Laboratory. The disk is available from several sources including MTS Software, St. Louis, MO for $5 and PC-SIG, Sunnyvale, CA for $6. It also is available from the National Technical Information Service, Springfield, VA 22161; call 703/487-4600 for ordering information.

TILTMETER STUDIES IN COLORADO AND WYOMING

Scientists at the NIST-University of Colorado Joint Institute for Laboratory Astrophysics (JILA) have completed field studies of specially-designed tiltmeters in Erie, CO, and Yellowstone National Park, WY. Tiltmeters are highly sensitive devices which are sunk deep into the earth and which are designed to measure the slightest tilt in the earth's surface. They might be used, among other things, as early-warning predictors for earthquakes. The JILA scientists found good agreement between their measurements and measurements of earth tides on the Colorado plains but wide disagreements between these measurements in Yellowstone Park where the instruments were placed above a collapsed caldera. "Only near a fault zone in

Germany have comparably large tilt anomalies been observed," they report. For copies of two papers explaining their work, contact Fred McGehan, NIST, Division 360.2, Boulder, CO 80303.

NIST TESTING SMOKE CONTROL SYSTEMS

Do smoke control systems really protect building occupants from deadly fumes? NIST researchers are conducting the first known full-scale tests on these systems. Smoke is the killer in most fires, which each year take nearly 6,000 lives in the United States. The idea behind smoke control systems is to help protect life and property by containing or diverting the smoke. NIST's research results will be used to evaluate current guidelines for smoke control systems, including those developed in 1983 by NIST in conjunction with the American Society of Heating, Refrigerating, and Air-Conditioning Engineers (ASHRAE), Inc. The data also will be used to develop and validate computer models to predict fire and smoke movement through a building and the vulnerability of occupants to fire.

INDUSTRY COOPERATION SOUGHT FOR NEW IPM PROGRAMS

NIST scientists are seeking researchers in industry, universities, and other organizations who are interested in participating in collaborative programs on the intelligent processing of materials (IPM). The IPM concept is a new computer-based approach for producing advanced polymer, ceramic, and metal alloy materials that are far superior to those used today. An IPM facility with on-line nondestructive evaluation (NDE) sensors and process models can carefully monitor and control the processing conditions required to give advanced materials their special properties. Currently, there are two IPM pilot demonstrations at NIST: researchers are working to automate the production of metal powders by both high-pressure gas atomization and hot isostatic pressing. Plans call for IPM programs in polymers, ceramics, and the thermomechanical processing of metals. For information, contact the Office of Nondestructive Evaluation, NIST, B344 Materials Bldg., Gaithersburg, MD 20899; telephone: 301/975-5727.

NEW TECHNIQUE FOR MEASURING STRESS AND STRAIN

NIST scientists have developed a computer-controlled, optical technique for measuring deformations in materials. The system, which utilizes a laser, video cameras, and still photography, measures all three components of strain as well as rigid body rotations. The system can measure strains at 16,000 locations in a 2.5-in square grid in about 5 h. It currently is being used to study the initiation and growth of cracks in composite panels in conjunction with an automobile manufacturer. Several papers are available from Jo Emery, NIST, Division 104, Boulder, CO 80303; telephone: 303/497-3237.

MAKING MOVIES TO SIMULATE STRESS WAVES

Using supercomputers and computer-generated graphics NIST researchers are trying to understand better how new composite materials—particularly graphite epoxy—stand up under stress and strain. With sophisticated mathematical modeling techniques, they are able to simulate a stress wave moving through a piece of graphite epoxy and, for the first time, view the progression of this wave in three dimensions from different planes and perspectives. They developed a simulated block of graphite epoxy containing 80,100 elements. A sound wave was "passed through" the block, taking almost 3 h and using virtually all the supercomputer's memory. When the results of the computer simulation were compared with theoretical models, there was a difference of less than 2 percent. New numerical techniques have reduced the time to 40 s and use much less computer memory. Working with NIST are two computer graphics companies.

CLINICAL INSTRUMENTS CAN BE STERILIZED IN SECONDS

The time required to sterilize dental and medical instruments can be reduced from hours to seconds by an innovative process developed at NIST. The new method disinfects instruments completely in 30 s when they are treated by a microwave-generated gas plasma produced in a container that holds the instruments inside a conventional microwave oven. The new technique should help health-care professionals improve patient care, and it may reduce the damage to expensive instruments caused by repeated exposure to traditional sterilization methods. A patent application has been filed, and NIST scientists hope to work with industry to

develop a practical appliance in which a gas plasma can be used routinely in a health-care facility. For information, contact: Dr. Waldemar de Rijk, NIST, A143 Polymer Bldg., Gaithersburg, MD 20899; telephone: 301/975-6803.

PROTOTYPE SYSTEM DEVELOPED ON STRUCTURAL CERAMICS

NIST scientists have developed a prototype computerized database system of critically evaluated data on structural ceramics. Designed for personal computers (PCs), the current focus is on the physical, chemical, and performance properties of structural ceramics expected to have near-term applications for the design of heat exchangers, radiant tube heaters, and engine components such as valves. Users can specify a material by generic and trade name, by composition and microstructure, or by desired property values. For information on the PC prototype, which is now being field tested, contact: Dr. Ronald G. Munro, NIST, A256 Materials Bldg., Gaithersburg, MD 20899; telephone: 301/975-6119.

LOOKS ARE NOT EVERYTHING

Does a change in the appearance of paint, such as fading, chalking, or yellowing, mean the coating can no longer protect the base material? Not necessarily, found researchers in the NIST Center for Building Technology. For the past several years, NIST has been investigating ways to predict the "service life" of building materials, including coatings. Knowing how long a material will remain serviceable can help in selection and use and in developing cost-effective maintenance strategies. But no quantitative test method exists to predict durability of coatings, and questions have been raised whether changes in appearance can be used as early indicators that the coating is deteriorating. The NIST researchers concluded that changes in appearance are not necessarily related to changes in the protective properties of a coating. A report, Relationship Between Appearance and Protective Durability of Coatings: A Literature Review (NISTIR 88-4010), is available from the National Technical Information Service, Springfield, VA 22161 for $15.95. Order by PB #89-162598/AS.

1989 ANNUAL DIRECTORY PUBLISHED FOR NVLAP LABORATORIES

The 1989 Directory of NVLAP Accredited Laboratories (NISTIR 89-4056), lists 200 laboratories nationwide and abroad that are accredited by NIST for specific test methods in various fields of testing as of April 1, 1989. The current fields are acoustics; carpet; commercial products—paint, paper, plastic, and seals and sealants; computer protocols; construction testing services—concrete, cement, aggregates, soil and rock, admixtures, geotextiles, road and paving; personnel radiation dosimetry; electromagnetic compatibility and telecommunications; solid fuel room heaters; and thermal insulation. The laboratories are listed alphabetically by name, field of testing, and state. For information on NVLAP programs, including the new bulk asbestos analysis program, contact: National Voluntary Laboratory Accreditation, NIST, A124 Bldg. 411, Gaithersburg, MD 20899; telephone: 301/975-4016. Information also is available by computer on the NVLAP electronic bulletin board at 301/948-2058. Copies of NISTIR 89-4056 are available prepaid for $15.95 from the National Technical Information Service, Springfield, VA 22161. Order by PB #89-189278.

TIPS FOR UTILIZING TEM CELLS

Transverse electromagnetic (TEM) cells are used widely to establish a known electromagnetic field for susceptibility testing and antenna calibrations. A recent NIST publication offers theoretical information and some practical tips for using TEM cells. The report addresses mechanical requirements for positioning the test equipment inside the cell, problems associated with cables, single- frequency and multi-frequency measurements, and use of a computer system for automated measurements. Theory and Measurements of Radiated Emissions Using a TEM Cell (NIST TN 1326) is available from the Superintendent of Documents, U.S. Government Printing Office, Washington, DC 20402. The cost is $2.25; order by stock number 003-003-02932-7.

USING EMATs FOR WHEEL INSPECTION

For several years NIST, at the request of the Federal Railroad Administration, has studied ultrasonic detection of cracks in the treads and residual tensile stresses in the rims of steel railroad wheels. These defects are two main causes of wheel failure, with catastrophic consequences to personnel,

rolling stock, tracks, and schedules. NIST's research program has concentrated on using electromagnetic-acoustic transducers (EMATs) for the nondestructive evaluation of wheels. These noncontact devices are more reliable and easier to automate than conventional transducers. Two instruments under development at NIST should be an improvement on the visual inspection methods now used, which have unacceptably high error rates. One instrument can detect cracks as the wheels roll by, enabling more frequent and thorough inspections than is now feasible; the second performs quantitative stress determination while the wheel remains on the axle. A collection of seven papers published over the past 2 years, Report No. 18: Ultrasonic Railroad Wheel Inspection Using EMATs (NISTIR 88-3906), is available from the National Technical Information Service, Springfield, VA 22161, for $15.95. Order by PB #89-189229.

NIST, AIR FORCE, INDUSTRY CONDUCT OSI/ISDN TRIAL

NIST and six companies recently conducted a trial at Mather Air Force Base in California to demonstrate the use of OSI applications over an ISDN transport network. OSI—Open Systems Interconnection—standards provide a set of rules, known as protocols, which enables information processing devices to communicate with one another in a network. ISDN—Integrated Services Digital Network—is a telecommunications technology that makes it possible to send and receive voice, data, and image signals simultaneously over existing digital telephone lines. NIST will release the results of the trial this summer. The results are expected to show that off-the-shelf computer products from different manufacturers can be connected through a variety of communications technologies, including ISDN. NIST has been working with private industry—users and manufacturers—and other organizations to help overcome problems inhibiting the growth of both OSI and ISDN technologies in the United States.

PROCESS DEVELOPED TO REMOVE TWINS IN YBCO CRYSTALS

A new technique for removing the twins in yttrium-barium-copper-oxygen (YBCO) single crystals may help scientists to understand better the performance of high-temperature superconducting materials. Twins are the interchange of the crystallographic *a* and *b* axes of a single crystal that occurs during processing as the material cools. These defects may contribute to superconductivity, but they also are barriers to information on the structure and properties of materials. The detwinning process uses pressure and heat to align the *a* axis parallel to the direction of applied stress. By characterizing untwinned single crystals, scientists will be able to determine the *a/b* structural and property anisotropy or directionality, and the effects of twin boundaries on superconductivity. Polarized light, optical microscopy, and x-ray studies were used to verify the new technique. For a copy of a report on the NIST detwinning process, send a self-addressed mailing label to Dr. Frank W. Gayle, NIST, A153 Materials Bldg., Gaithersburg, MD 20899.

IGNITION OF STEEL IN OXYGEN ATMOSPHERES TESTED

Many high-strength alloys burn readily in pressurized oxygen atmospheres, a fact of interest to many in science and engineering, but of particular consequence to the aerospace community. For several years, NIST has conducted studies sponsored by NASA of the ignition and combustion of various iron-, aluminum-, nickel-, and cobalt-based alloys in oxygen. The purpose of the work is to gain a fundamental understanding of the ignition characteristics of broad classes of metals in oxygen atmospheres. The results of the latest tests on a stainless steel alloy (UNS S66286) are now available. The details of the tests are presented in Ignition Characteristics of the Iron-Based Alloy UNS S66286 in Pressurized Oxygen (NISTIR 88-3904), available from the National Technical Information Service, Springfield, VA 22161, for $13.95 prepaid. Order by PB #89-189336.

RESEARCH RECOMMENDED TO IMPROVE OIL SPILL RESPONSE

Research, new tests, and improved techniques are needed to advance oil spill response capabilities in the Arctic, concludes a panel of experts in a recently issued NIST report. These findings were reached at a November 1988 workshop, which was coordinated by NIST for the Minerals Management Service of the U.S. Department of the Interior. It was held to discuss all aspects of oil spill response under Arctic conditions, to describe existing research programs, and to identify future research needs and priorities. Among the recommendations is that additional research, including field testing, is needed to evaluate combus-

tion of oil spills on water. The NIST Center for Fire Research is conducting laboratory tests to measure burning rate, smoke emission and movement, and particulate deposition. A report, Alaska Arctic Offshore Oil Spill Response Technology Workshop Proceedings (NIST SP 762), is available from the Superintendent of Documents, U.S. Government Printing Office, Washington, DC 20402. Order by stock no. 003-003-02935-1, for $11 prepaid.

COMPOSITION OF EARTH STUDIED WITH CUSTOM TECHNIQUE

Using a custom-made chemical measurement system, researchers at NIST are helping to unlock secrets about the earth's composition, evaluating the origins of precious metal ores, and determining the contributions of extraterrestrial material to the earth's makeup. At the heart of the NIST-developed system is a powerful technique known as resonance ionization mass spectrometry (RIMS). Among other things, RIMS enables scientists to measure rhenium and osmium, two difficult-to-detect elements found in the earth's rocks. By gauging the abundance of these two elements in a rock sample, scientists can determine the age of a rock and learn much about the history of the earth at the site where the sample was taken. The RIMS technique of measuring rhenium and osmium has been used successfully in studies that examine how deposits of platinum, gold, and other precious metals were created. For example, the method played a key role in a study showing that the movement of water mobilized certain components of very old rocks, creating gold deposits in the Kolar Region of India. RIMS also has been employed for other types of chemical analyses, such as measuring impurities in the thin films that coat semiconductors.

NEW DEVICE SAVES ELECTRONIC COMPONENTS

A new instrument that non-destructively tests electronic switching components has been developed by a NIST electronics engineer. The instrument—an automated power transistor switching test system—determines the maximum voltage and current levels that the device under test can switch without destroying it. The idea behind the new instrument is that the temperature rise which actually destroys the transistor, or other power electronic device, occurs slightly after the electrical breakdown of the device. The breakdown occurs when the electric current reaches a point where the device can no longer stand the voltage in the circuit. The trick is to remove the power before the device heats up enough to be damaged. Knowing the performance limits of transistors can reduce a user's costs because users often make their transistor specifications more stringent than necessary to ensure system reliability. Power transistors are vital components in control systems for applications ranging from the main engines of the space shuttle to your automobile. They are essential to electronic amplifiers, modern switching power supplies, and electric motor drives.

NIST PROBE ADAPTED FOR COMMERCIAL USE

A tiny, broadband electric field probe designed, tested, and calibrated by NIST engineers has been adapted into a commercial product. The probes are used for electromagnetic interference testing and non-ionizing radiation hazard measurements. NIST developed ultra-broadband resistively loaded dipoles and used the Denver Research Institute, Denver, CO, to provide the sensor element. NIST fabricated an ultra-broadband electric field probe using these dipole elements, which can measure fields of 1 to 1600 V/m over a range of 100 kHz to 18 GHz. NIST first announced development of the probe in the IEEE Transactions on Microwave Theory and Techniques, February 1987, in a paper titled "An Isotropic Electric-Field Probe with Tapered Resistive Dipoles for Broadband Use, 10 kHz to 18 GHz." For a copy of the original NIST paper, contact Dr. M. Kanda, NIST, Division 723.03, 325 Broadway, Boulder, CO 80303; telephone: 303/497-5320.

Standard Reference Materials

NEW MATERIAL CAN HELP GAUGE SULFUR EMISSIONS

Two new standard reference materials (SRMs 2730 and 2731), developed to help ensure that laboratories make accurate analyses of sulfur emissions produced by U.S. pulp and paper industries, are now available from NIST. The SRMs are intended for calibrating laboratory instruments and for evaluating the methods used for determining the concentration of hydrogen sulfide emitted into the atmosphere. Supplied in aluminum cylinders, the SRMs represent two concentrations of hydrogen

sulfide: 5 and 20 parts per million. The materials cost $730 per cylinder and may be ordered from the Office of Standard Reference Materials, NIST, B311 Chemistry Building, Gaithersburg, MD 20899; telephone: 301/975-6776.

STANDARD REFERENCE MATERIAL 1845—CHOLESTEROL IN WHOLE EGG POWDER

The Office of Standard Reference Materials announced the availability of Standard Reference Material (SRM) 1845, Cholesterol in Whole Egg Powder. This SRM is intended primarily for use in developing and validating analytical methods for the determination of cholesterol in an egg or other food matrix.

NIST obtained commercially the dried whole egg powder for SRM 1845 from M. Ihnat, Land Resource Research Centre, Agriculture Canada. The certified concentration for cholesterol in this material as provided in the Certificate of Analysis is 19.0±0.2 mg/g. This certified concentration and associated uncertainty was derived from data generated at NIST from a definitive method for cholesterol based upon isotope dilution gas chromatography/mass spectrometry. Details of the analytical methodology including extraction procedures are given in the Certificate of Analysis.

One of the effects of dietary factors on disease being studied is the relationship of increased cholesterol to heart disease. Since egg is an important source of cholesterol in the diet, this SRM should assist investigators in developing more accurate data for the concentration of cholesterol in egg and other foods.

Standard Reference Data

A NEW METHOD FOR IDENTIFICATION OF SOLID-STATE MATERIALS

The Crystal Data Center has developed a highly accurate analytical procedure that will greatly extend identification techniques, particularly for electron diffractionists. The method opens new opportunities in the identification of solid-state materials, in that crystalline samples in the size range 10 μm to 10 Å can be accurately characterized.

Research with NIST CRYSTAL DATA (a large database with chemical, physical, and crystallographic data on solid-state materials) has proved that a material can be uniquely characterized on the basis of its crystal lattice and chemical composition. To characterize a material, it is sufficient to determine the primitive cell and to determine the element types present. Using a modern analytical electron microscope (AEM), the experimentalist can collect the required data on an unknown sample. The lattice information is obtained by rotation of the sample to obtain two planes of data, from which a unit cell defining the lattice can be deduced. The chemical data is determined by energy dispersive x-ray spectroscopy (EDS). Once the experimental data are measured, the unknown can be identified against the database of knowns using well-developed lattice/element-type matching techniques.

Rapid and accurate identification of the unknown against lattices in the database with 140,000 entries is due: 1) to the development of a universal classification scheme for all lattices independent of crystal system and lattice centering; 2) to theoretical work that has led to algorithms that can deduce the relationship, if it exists, between any pair of lattices; and 3) to the creation of computer algorithms and search software to carry out lattice matching in a highly efficient manner when an extremely large number of lattices are involved.

Plans are under way to build this procedure directly into the workstations associated with commercial analytical electron microscopes, through technology transfer with private-sector groups. This strategy, then, provides an automated identification technique since data collection, NIST CRYSTAL DATA, and the identification software will all be integrated into the same instrument. The methodology is also useful for the identification of unknowns by means of neutron and x-ray diffraction data.

Volume 94, Number 5, September–October 1989
Journal of Research of the National Institute of Standards and Technology

Calendar

August 16–21, 1990

INTERNATIONAL CONFERENCE ON THE CHEMISTRY OF ELECTRONIC CERAMIC MATERIALS

Location: Grand Teton
National Park, WY

Materials chemistry has evolved from the more identifiable disciplines of inorganic and solid state chemistry, ceramics and materials science. It is inherently interdisciplinary, attracting scientists from many different backgrounds, such as materials science, physical, inorganic and organo-metallic chemistry, physics, ceramics, and mineralogy. This conference will bring together major national and international researchers to bridge the gap between those primarily interested in the pure chemistry of inorganic solids and those interested in the physical and electronic properties of ceramics. One of the primary goals of the conference will be to evaluate our current understanding of the chemistry of electronic ceramic materials and to assess the state of a field that has become one of the most important areas of advanced materials research. Sponsored by NIST together with the Office of Naval Research and other scientific organizations—federal, university, and industry.

Contact: Robert Roth, B126 Materials Building, NIST, Gaithersburg, MD 20899, 301/975-6116.

February 5–8, 1990

FOURTH INTERNATIONAL SYMPOSIUM ON BIOLOGICAL AND ENVIRONMENTAL REFERENCE MATERIALS BERM-4

Location: Sonesta Village Hotel
Orlando, FL

The Fourth Symposium will continue the series being held on an approximate 2-year periodic basis. The excellent exchange of ideas and views documented in the Proceedings of the Third Symposium, held in May 1988 at Bayreuth, Bavaria, FRG, covered a wide variety and scope of information in this topical area. Activities at the Fourth Symposium are expected to both broaden these discussions and to focus on more specific aspects of further research on problems and progress of projects discussed at the previous symposium. The major aim of this symposium series is to bring together efforts in the production, study and use of these reference materials in the analytical, biological, biomedical, clinical, environmental, and nutritional communities.

Contact: Wayne R. Wolf, B311 Chemistry Building, NIST, Gaithersburg, MD 20899, 301/975-2030.